Chapter–5

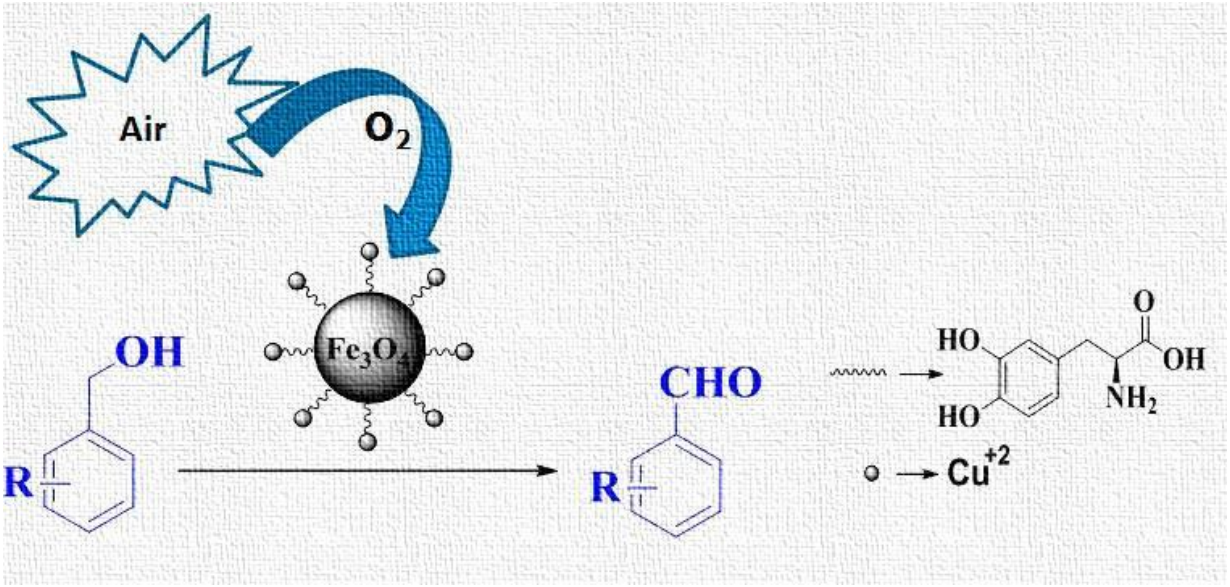

Nanoparticle–supported and magnetically recoverable organic–inorganic hybrid copper (II) nanocatalyst: a selective and sustainable oxidation protocol

Published in *RSC Advances, 2014, 4, 41111*

5.1 Introduction

The selective oxidation of alcohols to their corresponding carbonyl compounds is one of the most useful reactions in industrial processes.[1] Oxidation reactions are usually difficult and typically require stoichiometric amounts of toxic heavy-metal salts or expensive catalysts involving noble metals such as gold, ruthenium, rhodium or palladium.[2–5] Traditionally, non-catalytic methods with stoichiometric, toxic, corrosive and expensive oxidants such as permanganate, dichromate and peroxy acids under stringent conditions of high pressure and/or temperature have been widely used for alcohol oxidation.[6–9] These reactions are also often carried out with high concentrations of bases and environmentally unfriendly organic solvents. Therefore, much attention has been paid to the development of heterogeneous catalytic systems that use clean and atom efficient oxidants like molecular oxygen or H_2O_2 without organic solvents.[10–13] Among them, the solvent-free aerobic oxidation of alcohols using molecular oxygen or air as the oxidant has become more attractive,[14–16] due to positive effects in terms of cost, safety and environmental impact. In this study, the objective is to develop an efficient catalytic system for the aerobic or H_2O_2 oxidation of various alcohols under solvent-free conditions.

The copper-catalyzed oxidation of organic compounds has attracted significant attention in recent years[17] owing to the high demand for mild and efficient oxidation catalysts.[18] Copper is an abundant metal in the Earth's crust and its redox properties make it ideally suited for catalytic oxidation processes, provided that the electron-transfer processes can be controlled by an appropriate ligand set. Therefore, a number of copper catalyzed aerobic oxidation systems have been well-established.[19] They employ copper salts in combination with 2,2,6,6-tetramethyl-piperidyl-1-oxy (TEMPO),[20] and various N ligands such as 2,2′-bipyridine (Bpy),[20c,h] 1,4-diazabicyclo[2.2.2]octane (DABCO),[20g] and 4,4′-trimethylene-dipyridine (TMDP).[20f] However, they are homogeneous[20] in nature and additional base is often needed,[20c, d, h] which limits their application in the oxidation of the base sensitive alcohols.

Magnetic nanoparticles (e.g. Fe_3O_4) have been extensively investigated as an inorganic support for the synthesis of organic–inorganic hybrid materials. They are potential

alternatives to conventional materials, being robust, readily available, high-surface-area heterogeneous catalyst supports.[21] They offer an added advantage of being magnetically separable, thereby eliminating the requirement of catalyst filtration after completion of the reaction. Most importantly when magnetic nanoparticles are used as supports, the size of the support materials decreases to the nanometer scale, and all of the catalytic sites on the external surface of the particles can be accessible to the substrates.[22]

Modified magnetic nanoparticles have been utilized as support for the incorporation of different transition metal ions.[23] However, most of these techniques require several reaction steps to introduce functional groups to the magnetic surface and often involves use of organosilica precursors as an organic shell to prepare a suitable support for trapping the metal ions.[24] The later are not only very expensive and toxic, but also involve complicated synthesis methods. Therefore, from both environmental and economic points of view, the preparation of modified magnetic nanoparticles via a simple method and without using organoalkoxysilane compounds is highly desirable. Although Fe_3O_4-containing high performance catalysts for the oxidation of alcohols are reported,[25] the application of copper metal catalysts based on modified magnetic nanoparticles as heterogeneous catalysts in the oxidation of alcohols is not reported.

In continuation of our efforts towards the development of efficient nanoparticle assisted catalysis[26] herein, an Fe_3O_4/ L-3,4-dihydroxyphenylalanine(LD) nanocomposite containing Cu^{+2} ions (Fe_3O_4-LD-Cu) was prepared via a simple method as a novel heterogeneous magnetic catalyst. The main goal of this catalytic synthesis was to introduce a novel and efficient readily available copper as effective catalyst, based on organic molecule-grafted magnetic nanoparticles to expand the use of these types of nanocomposites for catalytic oxidation reaction. Literature survey reveals that this type of catalytic system is less reported[27] for the aerobic and H_2O_2 oxidation of alcohols. Initially benzyl alcohol was used as the model system to simplify the analysis and to accelerate the screening speed. Consequently the optimized conditions were used for the synthesis of various aromatic aldehydes.

5.2 Experimental

5.2.1 Materials

Benzyl alcohol, other alcohols, $FeCl_3 \cdot 6H_2O$, $FeCl_2 \cdot 4H_2O$, Ammonium hydroxide, $Cu(NO_3)_2.3H_2O$, TEA, H_2O_2, Ethanol, and L-3,4-dihydroxyphenylalanine (LD) were purchased from Merck Mumbai, India. All the solutions were prepared using double-distilled and demineralized water.

5.2.2 Synthesis of magnetic nano-ferrites

Fe_3O_4 nanoparticles were synthesized by a co-precipitation method as reported previously.[28] $FeCl_3 \cdot 6H_2O$ (6.95 g) and $FeCl_2.4H_2O$ (10 g) were dissolved in 50 mL of deionized water and stirred at 50 °C for 30 min under a nitrogen atmosphere. Then, ammonium hydroxide (25 %) was added slowly to adjust the pH of the solution to 10. The reaction mixture was then continually stirred for 1 h at 60°C. The precipitated nanoparticles were separated magnetically, washed with water until the pH reached 7, and then dried under vacuum at 60 °C for 2 h. This magnetic nanoferrite (Fe_3O_4) was then used for further chemical modification.

5.2.3 Surface modification of nano-ferrites

Nano-Fe_3O_4 (1 gm) was dispersed in 10 mL water by sonication for 30 min. L-DOPA (1 gm) dissolved in 5 mL of water was added to this solution and again sonicated for 2 h. The amino acid functionalized nanomaterial was then isolated by external magnet, washed with water and dried under vacuum at 60° C for 2 h.

5.2.4 Synthesis of nano- Fe_3O_4-L-DOPA-Copper complex (Fe_3O_4-LD-Cu)

Amino acid functionalized nano-Fe_3O_4 (1 gm) was dispersed in water-ethanol mixture (1:1). To this an aqueous solution of $Cu(NO_3)_2.3H_2O$ (120 mg) was added. Triethyl amine (TEA) solution in water was added drop wise to bring the pH of this mixture to 6. The reaction mixture was then stirred for 24 h at room temperature. The product was allowed to settle, washed several times with water and acetone, and dried under vacuum at 60°C for 2 h.

5.2.5 Details of Experimental Procedure for Fe_3O_4-LD-Cu Catalyzed Oxidation of Alcohol

5.2.5.1 H_2O_2 as oxidant- Benzyl alcohol (10 mmol) was heated with 30% v/v H_2O_2 (11 mmol) at 70°C in presence of 25 mg (0.02 wt% or 0.003 mmol copper by AAS) of Fe_3O_4-LD-Cu catalyst and stirred at that temperature for 4 h. The progress of reaction was monitored by thin layer chromatography (TLC). On completion of the reaction the mixture was cooled to room temperature and the catalyst was removed by an external magnet. The liquid organic product was analysed by gas chromatograph to calculate benzyl alcohol conversion and benzaldehyde selectivity. For isolation, the product was extracted with ethyl acetate. The combined organic layer was washed with water and brine solution and finally dried over anhydrous Na_2SO_4. Evaporation of solvent left the crude benzaldehyde with 96% selectivity, which was purified by column chromatography over silica gel (ethyl acetate:hexane 5:95 v/v) to provide pure benzaldehyde in 87% yield. Oxidation of other alcohols was carried out in a similar manner.

5.2.5.2 Air oxygen as oxidant- In a typical reaction, benzyl alcohol (1 mL, 10 mmol) and the magnetic catalyst (25mg) were loaded in a two-neck round bottom flask. The mixture was then exposed to air for oxygen flow into the mixture to initiate the reaction. Afterwards, the reaction mixture was stirred under solvent-free conditions with air oxygen for 4.5 h. Conversion and selectiviyty were determined by GC. The product was isolated by following the similar workup as above. Oxidation of other alcohols was carried out in a similar manner. In case of solid reactants acetonitrile was used as a solvent.

All experiments have been repeated three times and the reproducibility confirmed. The products purified by short-path silica gel chromatography (0–25% ethyl acetate in hexane, v/v) were analyzed by gas chromatography (GC) and ^{1}HNMR spectroscopy. The recyclability of the NPs was also surveyed. The NPs were recovered by magnet and washed with water followed by methanol and again water. They were dried at 60 ºC under vacuum and used directly for the next round of reaction without further purification.

5.2.6 Characterizations methods

The amount of copper in the catalyst and in the supernatant was estimated by atomic absorption spectroscopy (AAS) on a AA 6300: Shimadzu (Japan) atomic absorption spectrometer using an acetylene flame. The optimum parameters for Cu measurements are: wavelength =324.7 nm; lamp current = 2 mA; slit width = 0.2 nm; fuel flow rate = 0.2 L min^{-1}. The powered X-ray diffraction (XRD) patterns were recorded with a PanAlytical (model; Empyrean) 'X'PERT-PRO XRPD of Cu Kα radiation (λ= 0.15406 nm) on advance X-ray power diffractometer. Samples were prepared by pressing dried powder and patterns were collected with scanning rate of 2°/min and 2θ ranging from 0 to 80°. Surface area and porosity of the nanocatalyst were measured by a volumetric adsorption system (Micromeritics Instrument corporation, USA, model ASAP 2010) using N_2 adsorption/desorption isotherms at 77 K upto 1 bar. Prior to the measurements, the samples were activated (degassed) by heating at the rate of 1 K/min upto 383 K under vaccum. The temperature as well as vacuum was maintained for 7 hours prior to the measurements. Surface area was calculated by Brunauer-Emmet-Teller (BET) method while the porosity by Barrett-Joyner-Halenda (BJH) method. High-Resolution Transmission Electron Microscopy (HR-TEM) was carried out using Jeol (Jem-2100) electron microscope operated at an acceleration voltage of 200 kV. For this purpose, dry powered sample was dispersed in methanol and ultrasonication treatment was given for 30 min. After that sample was deposited onto a carbon-coated grid at room temperature and it was allowed for air-drying (about 6 hours). Selected area electron diffraction patterns (SAED) and Energy-dispersive X-ray spectroscopy (EDX/EDS) were also investigated from the electron micrographs. FT-IR spectra were recorded as KBr pellet on Perkin Elmer RX1 model in the range of 4000-400 cm^{-1}. Magnetic measurements were done by a vibrating sample magnetometer (EG&G Model 155 VSM) at room temperature in the range +20,000 to −20,000 G. The surface composition was investigated using X-ray Photoelectron Spectroscopy (XPS) on VSW X-ray photoelectron spectrometer (UK) using Mg and Al twin anode X-ray gun with multichannel detector and hemispherical analyser having resolution of 1.0 eV. The

binding energies obtained in the XPS analysis were calibrated against the C1s peak at 284.6 eV.

Fe_3O_4-LD-Cu nanocatlyst catalyzed oxidation reaction was monitored on thin-layer chromatography (TLC) and gas chromatography (GC). All products of the reduction of nitroarenes are commercially available and were identified by comparing their physical and spectral data (m.p., TLC (silica gel 60 F254, Merck, Mumbai, India), GC (Perkin Elmer clarus 500 GC) and ^{1}H NMR (BRUKER 400 MHz) with those of authentic samples or reported data.

5.3 Results and Discussions

5.3.1 Catalyst characterization

We used magnetite nanoparticles (Fe_3O_4), which were prepared by the co-precipitation method.[28] It was reacted with L-3,4-dihydroxyphenylalanine (LD) in water to yield the Fe_3O_4-LD, these obtained nanoparticles were further metallated with copper nitrate in ethanol to achieve the final copper complex grafted magnetically recoverable nanoparticles (Fe_3O_4-LD-Cu) (**Scheme 5.1**).

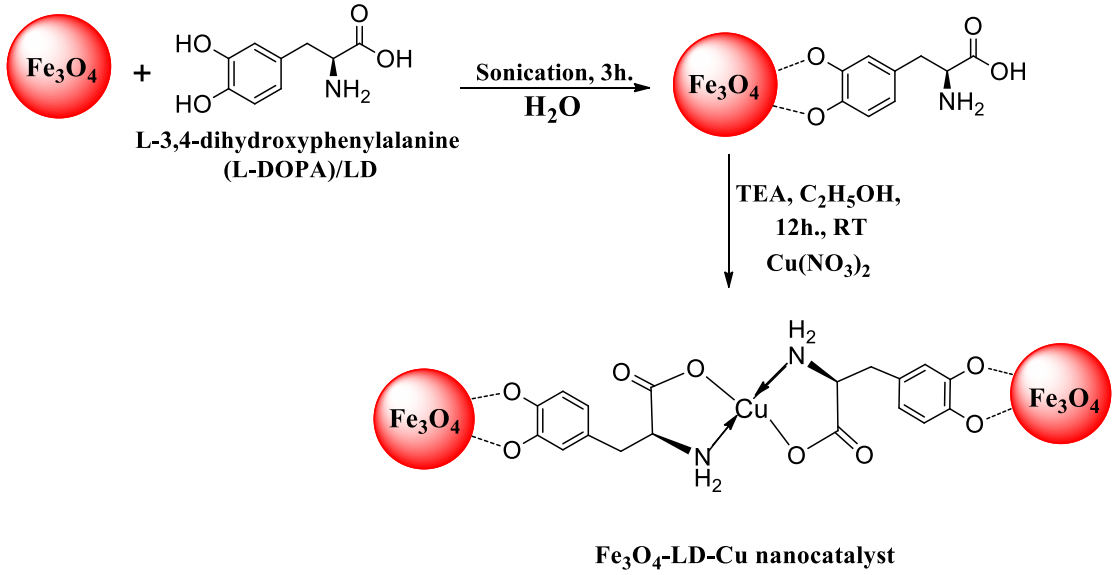

Scheme 5.1 Schematic representation of synthesis of Fe_3O_4-LD-Cu nanocatalyst

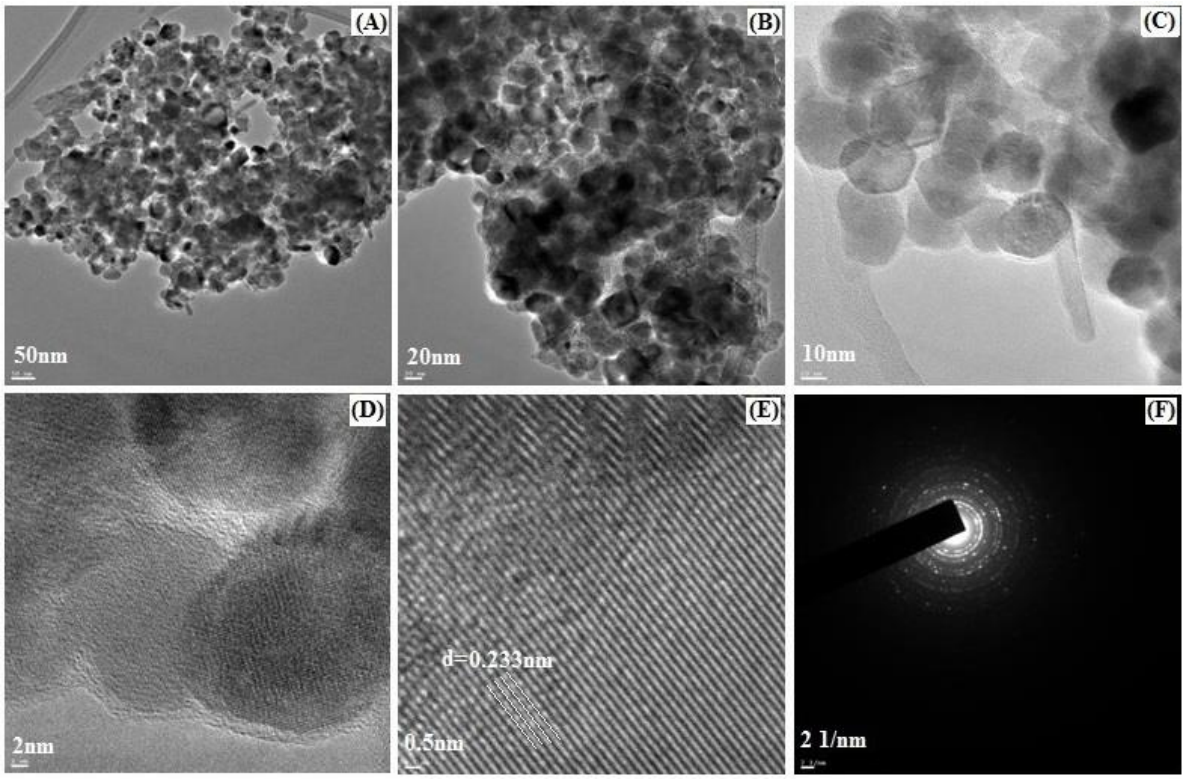

Figure 5.1 HR-TEM images of magnetic Fe_3O_4-LD-Cu nanocatalyst at different magnifications (A) 50nm (B) 20nm (C) 10nm and (D) 2nm showing particle size distribution; The resolved lattice fringes and SAED pattern of Fe_3O_4-LD-Cu are (E) and (F) respectively.

The High-Resolution Transmission Electron Microscopy (HR-TEM) images of Fe_3O_4-LD-Cu nanocatalyst are shows somewhat spherical morphology with some cubic partials an average size range of 20–30 nm (**Figure 5.1A**). **Figure 5.1B** and **C** are HR-TEM images of typical Fe_3O_4-LD-Cu at different magnifications. The nanoparticles, depicted in **Figure 5.1C** and **D** have a discrete core/shell structure, and their uniform magnetic core with a diameter of 10–15 nm is surrounded by a 2–3 nm thick LD organic shell. The high resolution images in **Figure 5.1E** shows well developed lattice fringes and the fringes extend throughout the particle confirming the monocrystalline nature of the individual particles. The distance between adjacent lattice fringes measured as 0.233nm in **Figure 5.1E** corresponds to the 311 reflection. The selected area electron diffraction

(SAED) pattern shown in **Figure 5.1F** corresponds to the higher order reflections of Fe_3O_4-LD-Cu nanocatalyst. The white spots as well as the bright diffraction rings indicate that the nanoparticles produced by the above stated method are highly crystalline.

The crystalline structures of Fe_3O_4, Fe_3O_4-LD and Fe_3O_4-LD-Cu were analysed by powder X-ray diffraction (XRD). As displayed in **Figure 5.2A to C**, all the samples show diffraction peaks at around 30.1°, 35.2°, 43.1°, 53.5°, 57.4° and 62.7° 2θ corresponding to the spinel structure of Fe_3O_4,[29] and which can be assigned to the diffractions of the (220), (311), (400), (422), (511) and (440) faces of the crystals, respectively. The relative intensities of the diffraction peaks matched well with the standard XRD data of Joint Committee on Powder Diffraction Standards (JCPDS) card number (19-0629) for Fe_3O_4 crystal as with a spinel structure, which is consistent with the TEM results. In addition, the XRD patterns depict similar diffraction peaks which indicate that the nanocomposite was synthesized without damaging the crystal structure of the Fe_3O_4 core. In addition, the broad diffraction peak in the range of 2θ between 10° and 30° can be attributed to the amorphous material coated on the magnetic nanoparticles.[30] According to the XRD results, it can be concluded that the Fe_3O_4 nanoparticles were successfully coated with LD and LD-copper. The XRD pattern clearly depicts that there is no change in the topological structure and inherent properties of Fe_3O_4 before and after the coating with LD. On assessment of the diffractograms of LD encapsulated and LD-copper complex grafted nanoparticles, the very distinguishable FCC peaks of magnetite crystal were not changed, which means that these particles have phase stability, but there is a slight decrease in intensity with broadening of the corresponding peak of LD (**Figure 5.2C**). It can be attributed to the lowering of scattering contrast between the walls of the Fe_3O_4 framework and organic moiety attached over Fe_3O_4. It also shows that different reaction conditions during the synthesis, did not affect the crystallinity and morphology of Fe_3O_4 nanoparticles throughout the process.

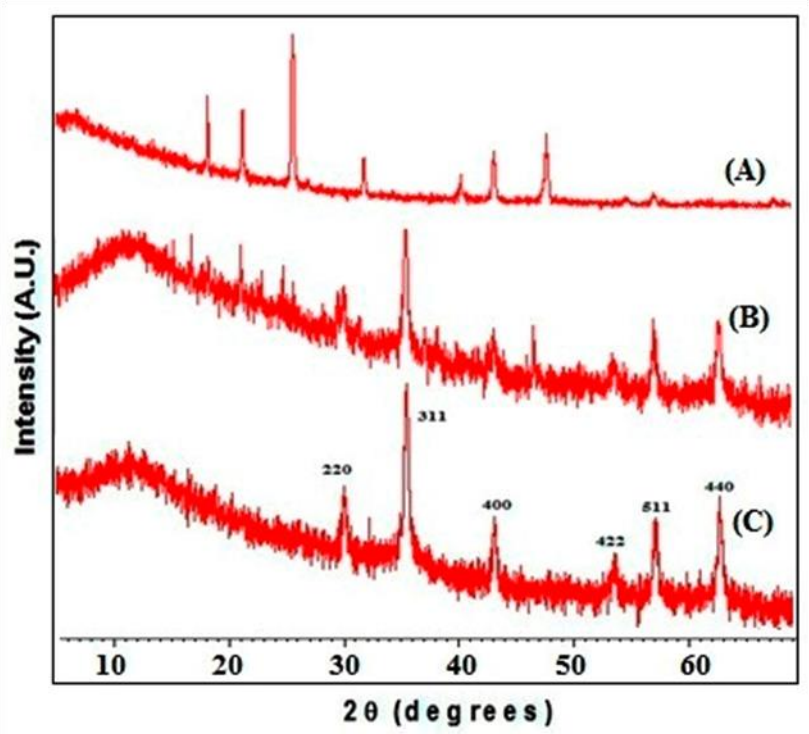

Figure 5.2 XRD pattern of (A) Fe_3O_4 (B) Fe_3O_4-LD and (C) Fe_3O_4-LD-Cu nanocatalyst

Fourier transform infrared spectroscopy (FT-IR) seems to be the best technique to characterize the functionalization and modification of magnetic nanoparticles. The FT-IR spectra of the LD, Fe_3O_4-LD and Fe_3O_4-LD-Cu nanocomposites were recorded to confirm the modification of the magnetite surface with the LD and metal ions (**Figure 5. 3A–C**). The IR spectra of LD (**Figure 5.3A**) is showing strong peak around 3404 cm^{-1} due to O–H stretching vibrations of catechol and 1652 cm^{-1} due to C=O stretching of carboxylic acids. The presence of magnetite nanoparticles in Fe_3O_4-LD is observable by the strong adsorption band at about 602 cm^{-1}, corresponding to the Fe–O vibrations (**Figure 5.3B**). It is also clear that the strong O–H stretching vibrations of catechol, which is generally present at 3400 cm^{-1}, is absent in the spectrum of Fe_3O_4-LD (**Figure 5.3B**). Instead, the broad band around 3106 cm^{-1} is seems due to O–H stretching of carboxylic acids. Moreover, on moving from LD to Fe_3O_4-LD, a significant reduction of the intensity of the O–H stretching and bending vibrations bands is observed. According to **Figure 5.3B**, the successful Fe_3O_4 surface modification with LD moieties has been

verified. In terms of Fe_3O_4-LD-Cu (**Figure 5.3C**), a red shift of the band at 1652 cm^{-1} is observed (1652 cm^{-1} → 1623 cm^{-1}), which is probably characteristic of the asymmetrical fluctuations of the carbonyl group after interaction with the metal ions. The band 3106 cm^{-1}, corresponding to the O–H bond stretching of carboxylic acids of LD (**Figure 5.3B**), intensity was decrease in the spectrum of the Fe_3O_4-LD-Cu (**Figure 5.3C**), indicating a strong interaction between the oxygen donors and the metal ions. The appearance of new bands in the region 575 cm^{-1} can be attributed to ν(M–N) while the stretching frequency bands in the 447 cm^{-1} region was correlated to ν(M–O), which confirmed the coordination through nitrogen and oxygen.[31] The FT-IR data confirmed that the nitrogen and carboxyl oxygen atoms are found to be involved in coordination with the metal ion in complexes. The IR results imply that Fe_3O_4-LD-Cu was successfully immobilized onto the surface of the magnetic nanoparticles.

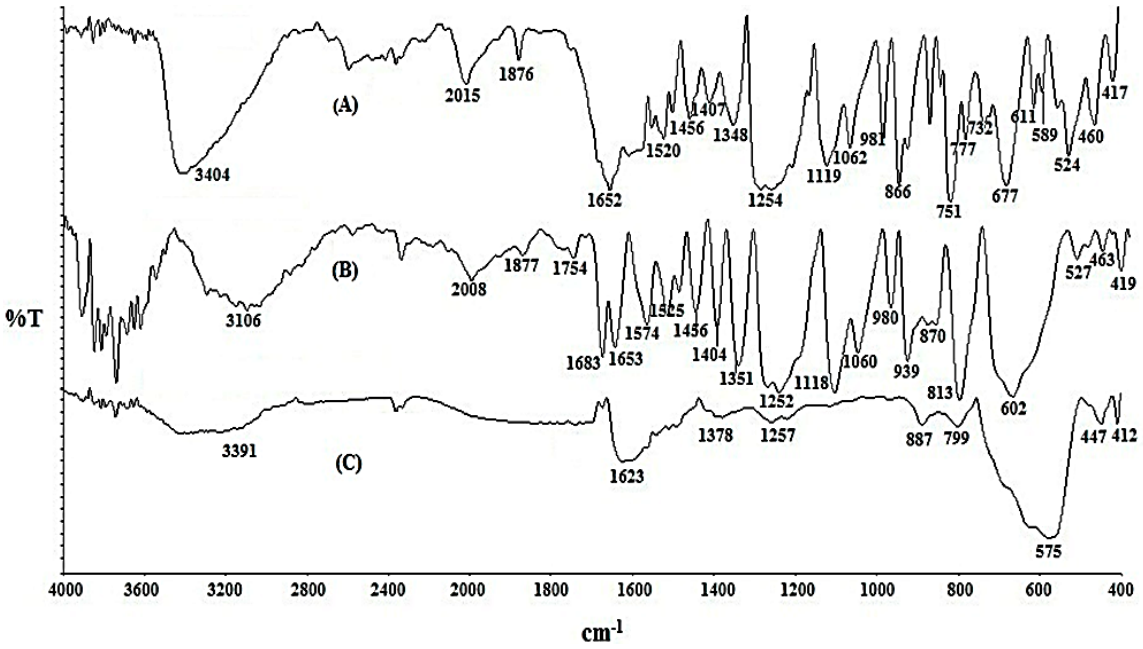

Figure 5.3 FT-IR spectra of (A) LD (B) Fe_3O_4-LD and (C) Fe_3O_4-LD-Cu nanocatalyst.

The weight percentage of copper content in the prepared nanocatalyst was performed using AAS, and sample digestions were carried out in a microwave oven at 500 watt for

10 min with a constant pressure programme with 5 mL aqua regia. The volume of the filtrate was then adjusted to 100 mL using double deionized water. Reference solutions for copper measurement were made with a high degree of analytical purity to obtain the calibration curves. 0.927% copper content in the catalyst was quantified using calibration curve in duplicate for each sample. Energy Dispersive X-ray Analysis (EDX) also confirm the ratio 1.20:98.80 (Cu/Iron oxide) (**Figure 5.4**). The EDX analysis of Fe_3O_4 nanoparticles are indicates that the well-cleaned final product is mostly composed of O, Fe (**Figure 5.4A**) and in the case of Fe_3O_4-LD-Cu nanocatalyst, O, Fe and Cu with no other signal in **Figure 5.4B**.

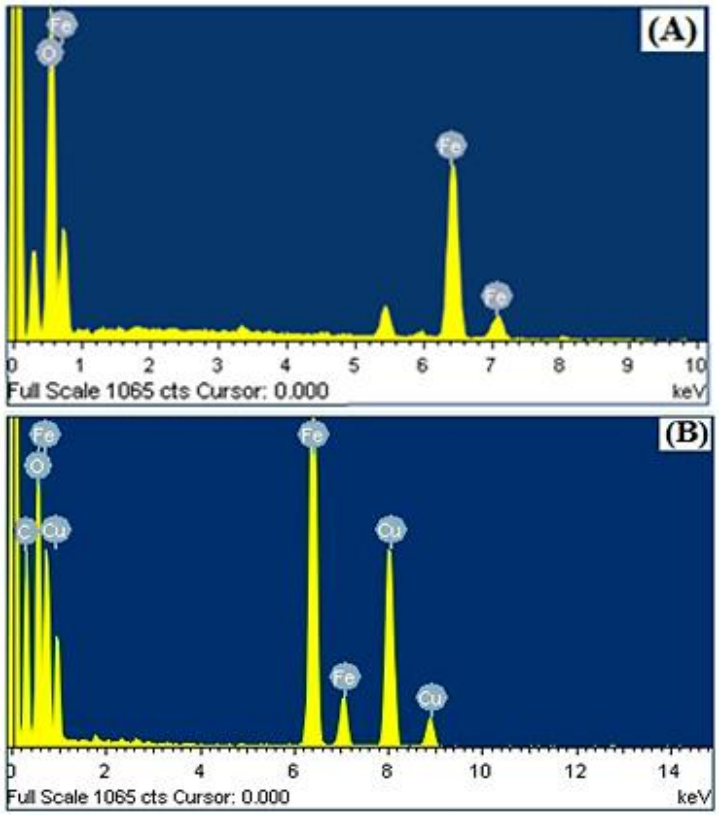

Figure 5.4 EDX patterns of (A) Fe_3O_4-LD and (B) Fe_3O_4-LD-Cu nanocatalyst

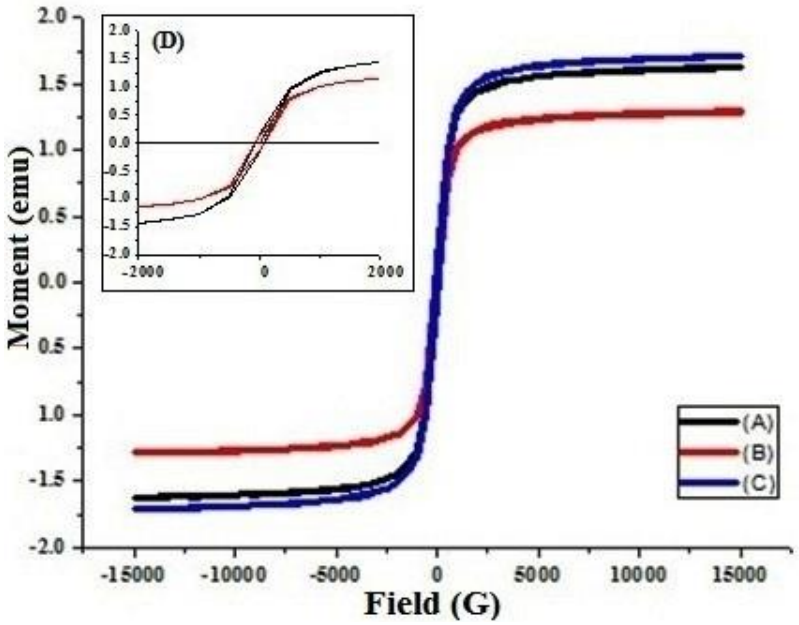

Figure 5.5 Magnetization curves obtained by VSM at room temperature for (a) Fe_3O_4 (b) Fe_3O_4-LD (C) Fe_3O_4-LD-Cu nanocatalyst and (d) inset: enlarged image near the coercive field.

The magnetic properties of the synthesized Fe_3O_4 nanoparticles, Fe_3O_4-LD and Fe_3O_4-LD-Cu were analyzed by vibrating sample magnetometry (VSM). The field-dependent magnetization curves shown in **Figure 5.5** indicate the magnetization as a function of applied magnetic field, measured at room temperature. The coercivity values of the Fe_3O_4 nanoparticles, Fe_3O_4-LD and Fe_3O_4-LD-Cu were 74, 73.65 and 71 G respectively. In spite of these low magnetization values with respect to magnetization of pure Fe_3O_4 nanoparticles,[23] which was owing to decrease in the surface moments of the magnetite nanoparticles by diamagnetic LD coating over Fe_3O_4 nanoparticles and grafting of metal–ligand complex over Fe_3O_4-LD, it is still sufficient for magnetic separation by a conventional magnet. The above mentioned TEM images also confirmed the encapsulation and grafting of the organic layer over Fe_3O_4 nanoparticles. Another important parameter for practical applications of nanoparticles is revealed from the enlarged VSM curve shown in **Figure 5.5D**. The hysteresis loops of powdered materials showed almost negligible magnetic hysteresis with both the magnetization and

demagnetization curves passing through the origin, which clearly indicates the super paramagnetic nature of the materials. This also means that the magnetic material can only be aligned under an applied magnetic field but, will not retain any residual magnetism upon removal of the field. Thus, the above discussed Fe_3O_4 nanoparticles appear to be suitable as the support for catalyst.

The Brunauer-Emmet-Teller (BET) surface area of a magnetic Fe_3O_4-LD-Cu sample was determined to be as high as 70.41 m^2/g, (**Figure 5.6 and 5.7**). Similarly, the BJH adsorption and desorption cumulative surface area of pores are 73.36 m^2/g and 73.06 m^2/g respectively (**Figure 5.8**). The Barrett-Joyner-Halenda (BJH) pore size of the NPs was determined to be 14.37 nm and the total pore volumes were 0.25 cm^3/g (**Figure 5.9**).

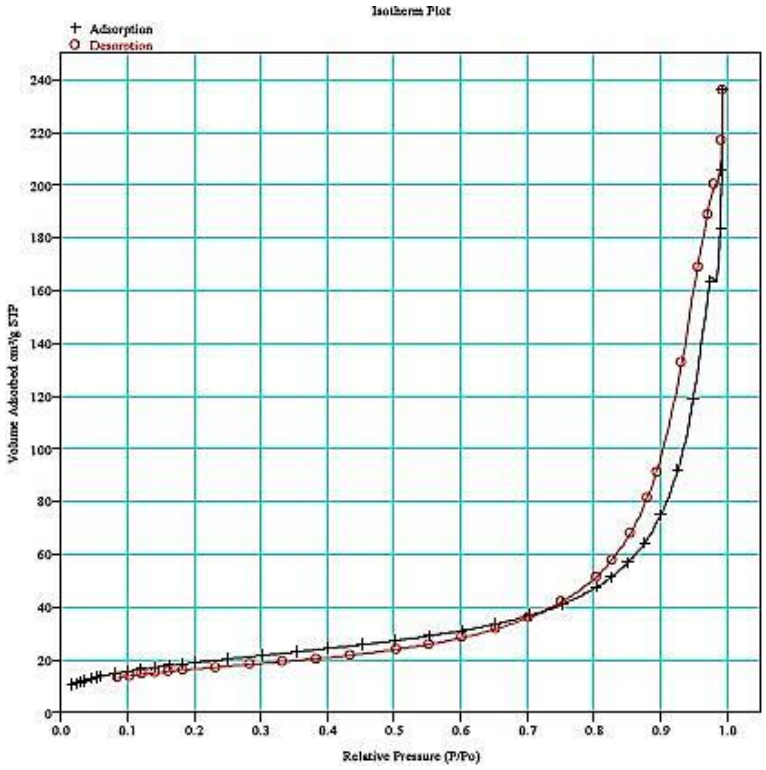

Figure 5.6 BET Isotherm Plot for Fe_3O_4-LD-Cu nanocatalyst

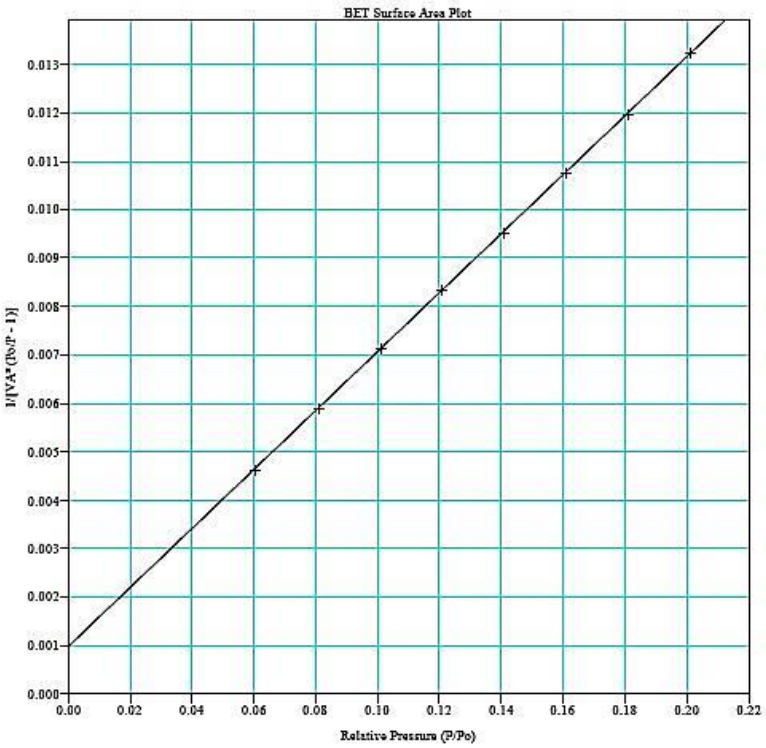

Figure 5.7 BET Surface area Plot for Fe_3O_4-LD-Cu nanocatalyst

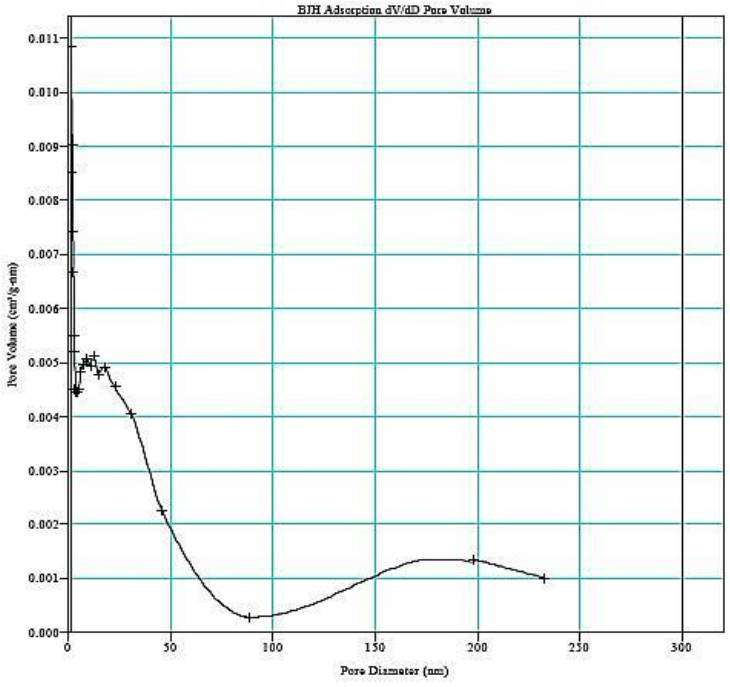

Figure 5.8 BJH Adsorption dV/dD Pore Volume for Fe_3O_4-LD-Cu nanocatalyst

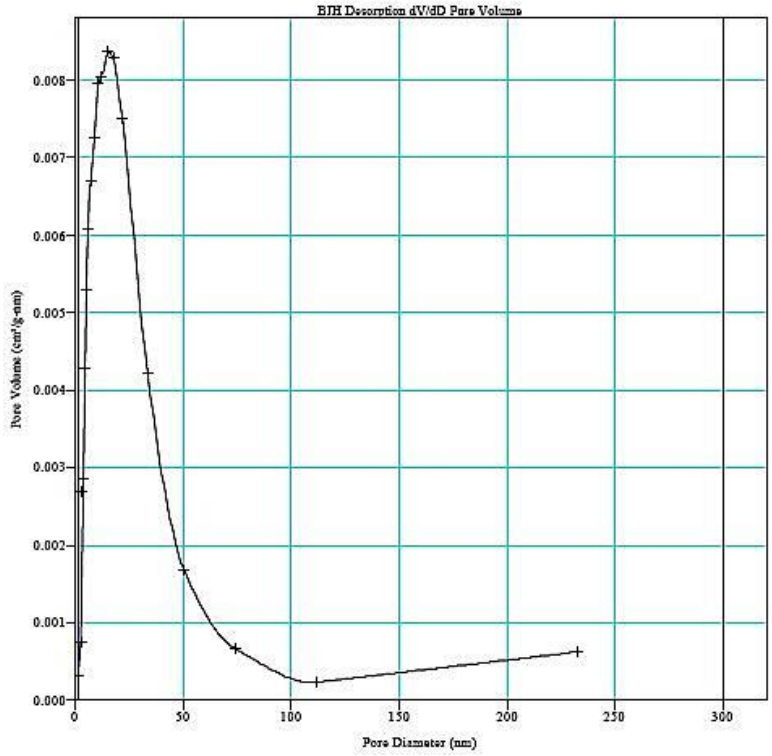

Figure 5.9 BJH Desorption dV/dD Pore Volume for Fe_3O_4-LD-Cu nanocatalyst

In order to provide further evidence of the formation of Cu^{2+} complex over the iron oxide core and to determine the oxidation state of copper, the XPS resolution copper 2p spectroscopy results of Fe_3O_4 and Fe_3O_4–LD–Cu were compared (**Figure 5.10A a and b**). The signals of Cu^{2+} were very faint in the XPS spectrum of the Fe_3O_4–LD–Cu nanocomposite (**Figure 5.10B**), because of the low loading of Cu^{2+} ions. Nevertheless, for a better understanding of the oxidation state of copper, the binding energy obtained from the catalyst was compared with the Cu^{2+} $2p_{3/2}$ and $2p_{1/2}$ peak positions. The binding energies of the main peaks are about 934.59 eV and 942.27 eV due to Cu $2p_{3/2}$ and Cu $2p_{1/2}$, respectively. Since these lie within the range given in literature,[32] it can be concluded that the oxidation state of copper in the catalyst is +2.

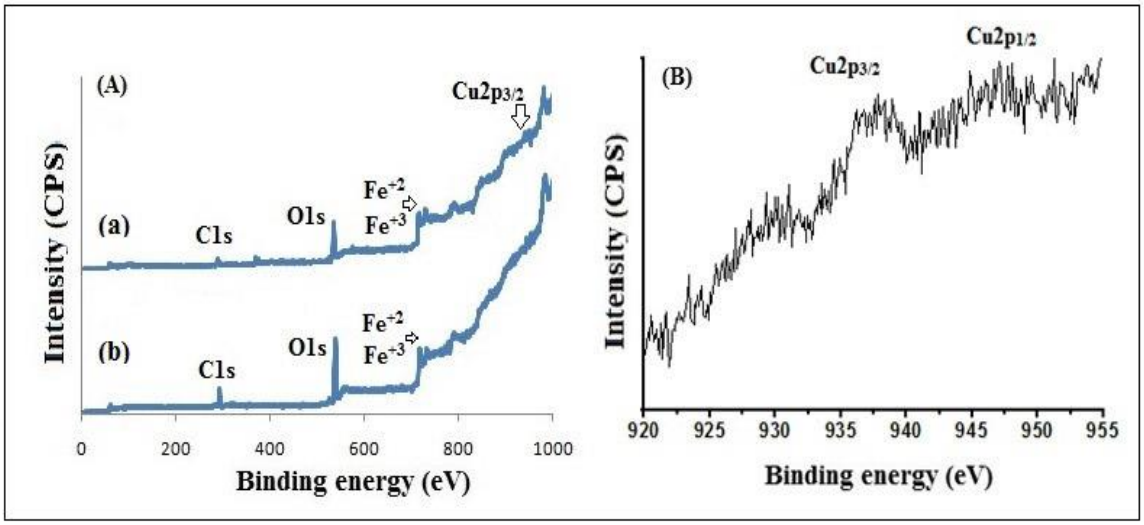

Figure 5.10 XPS analysis of (A) Fe_3O_4 and Fe_3O_4-LD-Cu nanocatalysts and (B) Expanded XPS region of Fe_3O_4-LD-Cu nanocatalysts

5.3.2 Catalytic activity

Having synthesized and characterized the Fe_3O_4-LD-Cu nanocomposite, its role as a heterogeneous catalyst was evaluated for the oxidation of alcohols. The oxidation was carried out with air as well as with H_2O_2 as oxidant. In order to optimize the reaction conditions and obtain the best catalytic activity, the oxidations of benzyl alcohol was chosen as a model reaction. In this regard, different reaction parameters such as solvent, temperature and amount of catalyst were investigated (**Table 5.1**).

It is seen from the **Table 5.1** (entry-1) that the presence of a catalyst is required for oxidation of benzyl alcohol. In order to investigate the role of Cu^{+2} in the catalyst, the model reaction was carried out under the optimized reaction conditions in the presence of Fe_3O_4 and Fe_3O_4-LD as catalyst (**Table 5.1**,entry-2). No progress in the reaction was observed even after five hours. Thus, it can be concluded that Cu^{+2} incorporated onto the magnetic nanocomposite plays a pivotal role in the solvent-free aerobic oxidation as well as H_2O_2 promoted oxidation of benzyl alcohol.

As far as the effect of solvent is concerned, the model reaction was performed in several solvents as well as in solvent free conditions (**Table 5.1**, entries-3 to7). It was observed that the best yield and selectivity were obtained when the reaction was conducted under solvent-free conditions (entry-8 and 9). Moreover, the effect of the catalyst amount on the oxidation of benzyl alcohol was also investigated by varying the amounts of the catalyst (**Table 5.1**, entries 8 to 10). As can be seen, while the amount of catalyst increased from 15 to 25 mg (entries 8 and 9), the product yield increased from 31% to 60% in air oxidation and 52 to 58 % in the H_2O_2 oxidation, which is probably due to the availability of more acid sites. Since then, the percentage yield remained stable between 25 mg to 50 mg catalyst, with a reduction of about 12% in benzaldehyde selectivity, which may be due to over-oxidation of the substrate at high amounts of the catalyst (entries-9 and 10). According to the results, 25 mg was chosen as the optimum amount of catalyst, due to the best yield and selectivity, for the further steps (**Table 5.1**, entry-9, Scheme-2).

The influence of reaction temperature on the catalytic activity was investigated by several separate reactions under the same reaction conditions. As represented in **Table 5.1**, in air oxidation the reaction yield is not increasing with temperature (entries-11, 12 and 14) but the selectivity to benzaldehyde decreased significantly because of over-oxidation at high temperatures.

In case of H_2O_2 oxidation of benzyl alcohol, when temperature increases from 25 to 70 °C (**Table 5.1**, entry-9 and 12), the reaction yield also increases from 58% to 95% with 96% selectivity of benzaldehyde. According to the results the reaction temperature of 25 °C and 70 °C appears to be the optimum reaction temperature for aerobic oxidation and H_2O_2 oxidation, respectively. According to above result in the **Table 5.1**, entries 9 and 12 are optimum condition for air and H_2O_2 oxidation of benzyl alcohol, respectively (**Scheme 2A and B**).

Table 5.1 Effects of different solvent, temperature and amount of catalyst on the aerobic and H_2O_2 oxidation of benzyl alcohol in the presence of Fe_3O_4-LD-Cu catalyst

Entry[a]	Temperature (°C)	Catalyst (mg)	Solvent	Air oxidation		H_2O_2 (30% V/V)	
				Conversion (%±2 by GC)	Selectivity (%±1 by GC)	Conversion (%±2 by GC)	Selectivity (%±1 by GC)
1	25-30	-	-	Trace	99	Trace	99
2	,,	Fe_3O_4/ Fe_3O_4-LD	-	20	99	35	92
3	,,	25	Water	12	88	30	70
4	,,	25	Ethanol	16	88	20	71
5	,,	25	Acetonitrile	49	99	48	94
6	,,	25	Dichloromethane	25	90	22	75
7	,,	25	Methanol	20	92	35	72
8	,,	15	Solvent-free	31	99	52	95
9	**,,**	**25**	**,,**	**60**	**99**	62	96
10	,,	50	,,	59	88	60	96
11	50	25	,,	58	85	72	96
12	**70**	**25**	**,,**	58	81	**95**	**96**
13	,,	50	,,	59	81	95	96
14	90	25	,,	60	80	95	91

[a]- Reaction conditions: benzyl alcohol (10 mmol), Benzyl alcohol: H_2O_2 (30% v/v) mole ratio = 1: 1.1, solvent=2mL, reaction time = 5 h, the main by-product was benzoic acid.

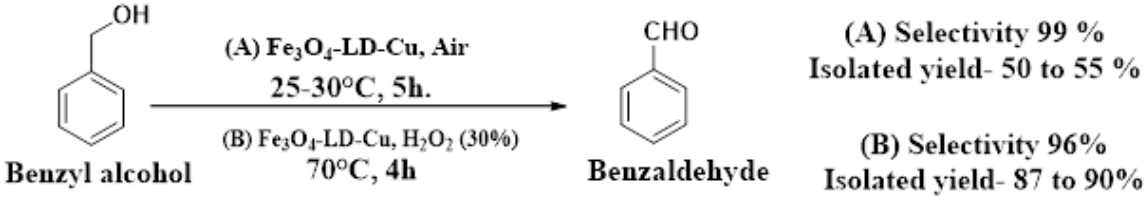

Scheme 5.2 Oxidation of benzyl alcohol to benzaldehyde in optimum reaction condition; (A) Air and (B) H_2O_2.

Table 5.2 Oxidation of Benzyl alcohol at different Benzyl alcohol /H_2O_2 ratios.[a]

Entry	Benzyl alcohol / H_2O_2(mmol)	T(h)	Yield(±1,by GC)
1	1:1	24	76
2	1:1.1	5	95
3	1:1.2	12	95
4	1:1.4	3.0	90
5	1:1.5	1.5	90
6	1:2	0.5	90

(a) All reaction carried out at 70° C by using Fe_3O_4-LD-Cu nanocatalyst (25 mg).

Table 5.3 Yield of product at different time interval by oxidation of Benzyl alcohol to benzaldehyde

Entry	Air oxidation[a]		H_2O_2 oxidation[b]	
	T (h)	Yield(±1, by GC)	T (h)	Yield(±1, by GC)
1	0.5	30	0.5	40
2	1	35	1	56
3	1.5	42	1.5	68
4	2	45	2	75
5	2.5	48	2.5	80
6	3	50	3	85
7	3.5	52	3.5	89
8	4	55	**4**	**96**
9	4.5	58	4.5	96
10	**5**	**60**	5	96
11	5.5	60	5.5	96
12	6	60	6	96

(a) All reaction carried out at 25-30 °C by using Fe_3O_4-LD-Cu nanocatalyst (25 mg) and air as oxidant. (b) All reaction carried out at 70 °C by using Fe_3O_4-LD-Cu nanocatalyst (25 mg) and H_2O_2 as oxidant (Benzyl alcohol: H_2O_2 (30% v/v) mole ratio = 1: 1.1)

In order to assess the efficiency of the NPs further, the quantity of H_2O_2 and reaction time were also optimized (**Table 5.2 and 5.3**). After optimization of the reaction conditions (**Table 5.1**, **5.2 and 5.3**), the catalytic activity of magnetic Fe_3O_4-LD-Cu nanocatalyst was further explored, with other benzylic alcohols.

Table 5.4 Aerobic and H_2O_2 oxidation of various benzylic alcohols over Fe_3O_4-LD-Cu nanocatalyst

Entry[c]	Reactant	Product	H_2O_2 (30% V/V)[a]		Air oxidation[b]	
			Conversion /TON	Selectivity	Conversion /TON	Selectivity
1	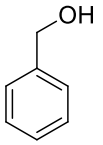	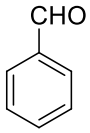	90/2500	96	52/1444	99
2	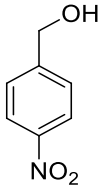	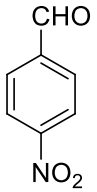	75/2083	79	36/1000	98
3	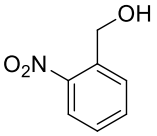	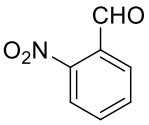	69/1916	89	30/833	98
4	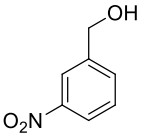	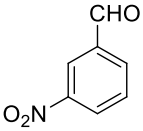	68/1888	92	40/1111	99
5	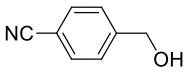	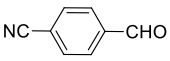	90/2500	96	59/1638	99
6	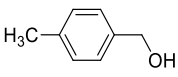	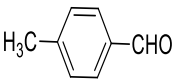	92/2555	98	62/1722	99
7	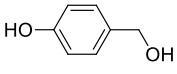	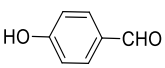	92/2550	95	61/1694	99
8	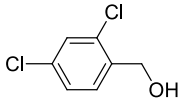	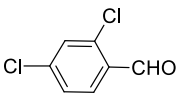	86 /2388	96	59/1555	99

9	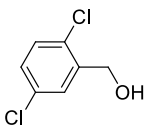	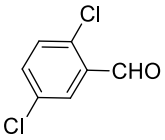	85/2361	96	60/1666	99
10	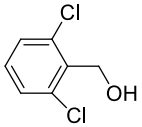	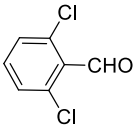	78 /2166	98	52/1444	99
11	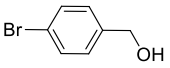	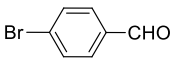	70/1944	92	49/1361	99
12	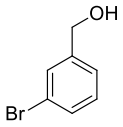	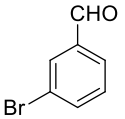	72/2000	95	52/1444	99
13	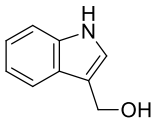	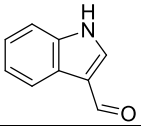	72/2000	96	47/1305	99

[a]-Reaction conditions: alcohol (10 mmol), atmospheric air, 25 mg catalyst (0.02 wt% or 0.003 mmol copper, obtained by AAS for Fe_3O_4-LD-Cu), reaction time and temperature, 12 h and 25-30 °C, respectively. Acetonitrile was used as a solvent (If alcohol is solid and air use as oxidant) = 2mL. [**b]-** Reaction conditions: alcohol (10 mmol), alcohol : H_2O_2 (30% v/v) mole ratio = 1 : 1.1, 25 mg catalyst, reaction time and temperature, 12 h and 70 °C, respectively.[**c]-**The main by-product was benzoic acid, TON was calculated on basis of Copper ion Estimated by AAS, Isolated yield after Column chromatography and Selectivity by GC.

The Fe_3O_4-LD-Cu catalyst exhibited good activity and selectivity in the solvent-free aerobic oxidation as well as by H_2O_2 oxidation of different benzylic alcohols (**Table 5.4**). All the investigated benzylic alcohols with either electron-donating or electron-withdrawing substituents can be oxidized into their corresponding aldehydes in high yields with excellent selectivity (entries 2−13). In all cases, the turnover number (TON) was as high as ~1850 to 2500 for H_2O_2 oxidation and ~830 to 1700 for air oxidation of various benzylic alcohols.

The recycling and recovery of used catalyst is one of the most important criteria of industrial based catalyst system, which gives useful information about the immobilization process and catalytic stability along the catalytic cycles. The reusability of the catalyst was tested by carrying out repeated runs of the reaction on the same batch of the catalyst in the model reaction (**Scheme 5.2 A and B**). In order to regenerate the catalyst, after each cycle, it was separated by an external magnet (**Figure 5.11A**) and washed several times with acetone. Then it was dried in an oven at 60 °C and reused in the subsequent run. The results show that this Fe_3O_4-LD-Cu magnetic catalyst can be reused seven times with no significant loss of activity/selectivity (**Table 5.5**). It should be mentioned that there was very low Cu^{+2} leaching during the reaction and the catalyst exhibited high stability even after seven recycles (**Table 5.5**). After that, however, the reaction time increased with each successive recycling experiment reaching from 5h to 6h finally in air oxidation. Similar result was also obtained in H_2O_2 oxidation of benzyl alcohol (**Table-5.5**). This may be due to gradual loss of the catalytic activity of the nanocatalyst with number of runs which may be due to various reasons. One of the reasons may be surface modification due to deposition of matter during reaction. The HR-TEM images of the nanocatalyst were recorded after 7^{th} run of air (**Figure 5.11B**) and H_2O_2 oxidation (**Figure 5.11C**) of benzyl alcohol. The HR-TEM images display an agglomeration of NPs due to deposited matter (**Figure 5.11B and C**).

It is evident from the **Table 5.6** that the Fe_3O_4-LD-Cu nanocatalyst is highly efficient in catalyzing the air as well as H_2O_2 oxidation of benzylic alcohols and gave products in good yields with high turnover number (TON) in comparison to the previous literature reports.[5,20e,f,23,25d,e] Hence, catalytic efficiency of the present catalytic system is remarkable in terms of mild reaction conditions, catalyst costs, short reaction time, high reaction yield and easy recovery of the catalyst.

Table 5.5 Air and H_2O_2 oxidation of benzyl alcohol to benzaldehyde over Fe_3O_4-LD-Cu nanocatalyst in optimum condition (Recycling experiments)

Cycle	Air oxidation[a]			H_2O_2 (30% V/V)[b]		
	Time (h)	Conversion (%±2 by GC)	Selectivity (%±1 by GC)	Time(h)	Conversion (%±2 by GC)	Selectivity (%±1 by GC)
1	5	60	99	4	95	96
2	5	59	99	4	95	96
3	5	60	99	4	94	95
4	5	59	98	4	95	95
5	5	58	99	5	94	94
6	6	59	99	5	94	95
7	6	58	99	6	94	96

[a]-Reaction conditions: alcohol (10 mmol), atmospheric air, 25 mg catalyst and reaction temperature 25-30°C [**b]** Reaction conditions: alcohol (10 mmol), alcohol:H_2O_2 (30% v/v) mole ratio = 1 : 1.1, 25 mg catalyst, reaction temperature 70 °C.

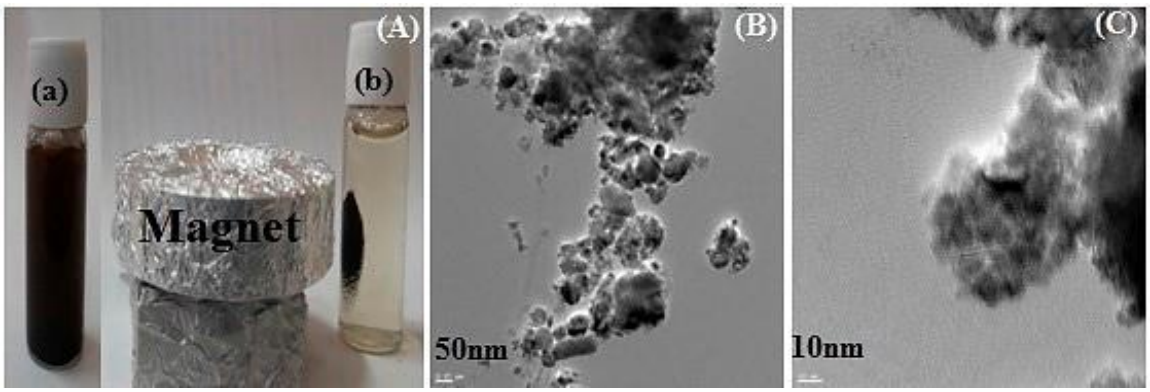

Figure 5.11 (A) Reaction mixture of benzaldehyde (a) before and (b) after magnetic separation by simple magnet; HR-TEM of reused magnetic Fe_3O_4-LD-Cu nanocatalyst after (B) Air oxidation and (C) H_2O_2 oxidation

Table 5.6 A comparison of the results of the present system with the recently published catalytic systems for the oxidation of alcohols to aldehyde.

entry	Catalytic system	Reaction conditions	% Yield by GC	Ref.
1	Fe_3O_4/MPA–PHEA-Cr composite	O_2-bubbling, 45 °C, 4h.	60	[23]
2	Cu-NHC-TEMPO	C_6H_5Cl, 80 °C, air, 15h.	70	[20e]
3	TEMPO/$CuCl_2$/bapbpy	*t*-BuOK, acetonitrile/methanol (2:1) ,rt, air,7 h.	18	[20f]
4	Nano-γ-Fe_2O_3	H_2O_2 , 75 °C, 12 h.	18	[25d]
5	polymer supported palladium catalyst	K_2CO_3, water, 100 °C, 6 h.	99	[5]
6	magnetically recoverable Au NP	Toluene, K_2CO_3, 100°C, Bubbling O2, 6h.	85	[25e]
7	Our catalyst	(a) Air, 25-30 °C, 5h. (b) H_2O_2, 70 °C, 4h.	(a) 60 (b) 96	This work

5.3.3 Hot filtration test

Hot-filtration based leaching test was conducted to exclude any homogeneous catalytic contribution or lixiviation of catalytic species in the catalyzed reaction. First, AAS analysis of the post reaction mixture after catalyst separation was conducted. The results revealed that the concentration of Cu(II) ions in the supernatant corresponds to negligible catalyst leaching (<0.01 ppm). There was hardly any change in the amount of Cu compared with the fresh catalyst.

5.4 Conclusion

In summary, a facile route to the synthesis of a copper containing Fe_3O_4/L-3,4-dihydroxyphenylalanine nanocomposite was reported without using any organosilane precursors. This catalyst was used for the oxidation of alcohols with high TON and excellent selectivity. Also, being magnetically separable, the requirement of catalyst filtration after completion of the reaction was eliminated, which is an additional sustainable attribute of this oxidation protocol. The magnetic catalyst exhibited high catalytic activity/selectivity in the solvent-free aerobic oxidation as well as H_2O_2 oxidation of alcohols.

5.5 Reference

1. a) R. A. Sheldon, I. W. C. E. Arends and A. Dijksman, *Catal. Today*, 2000, **57**, 157; b) P. J. Figiel, J. M. Sobczak and J. J. Ziólkowski, *Chem. Commun*, 2004, 244; c) T. Waters, G. N. Khairallah, S. A. S. Y. Wimala, Y. C. Ang, R. A. J. O'Hair and A. G. Wedd, *Chem. Commun*, 2006, **20**, 4503; c) S. Kodama, Y. Ueta, J. Yoshida, A. Nomoto, S. Yano, M. Ueshima and A. Ogawa, *Dalton Trans.*, 2009, 9708; d) A. Dewan, T. Sarma, U. Bora and D. K. Kakati, *Tetrahedron Lett.*, 2011, **52**, 256; e) S. Parihar, R. N. Jadeja and V. K. Gupta *RSC Adv.*, 2014, **4**, 10295 (f) C. Parmeggiani and F. Cardona, *Green Chem*,. 2012, **14**, 547; g) Z. Guo, B. Liu, Q. Zhang, W. Deng, Y. Wang and Y. Yang *Chem. Soc. Rev.*, 2014, **43**, 3480.
2. a) J. Muzart, *Tetrahedron*, 2003, **59**, 5789; b) J. Wang, X. Lang, B. Zhaorigetu, M. Jia, J. Wang, X. Guo and J. Zhao, *ChemCatChem*, 2014**, 6**, 1737.
3. H. Mimoun, M. M. Perez Machirant and I. Seree de Roch, *J. Am. Chem. Soc.*, 1978, **100**, 5437.
4. G. Csjernyik, A. H. Éll, L. Fadini, B. Pugin and J.-E. Bäckvall, *J. Org. Chem.*, 2002, **67**, 1657.
5. M. M. Dell'Anna, M. Mali, P. Mastrorilli, P. Cotugno and A. Monopoli, J *Mol Catal A: Chem*, 2014, **386**, 114.
6. R. A. Sheldon and J. K. Kochi, Metal-Catalyzed Oxidations of Organic Compounds, Academic Press, New York, 1981.
7. M. Hudlicky, Oxidations in Organic Chemistry, American Chemical Society, Washington, DC, 1990.
8. C. L. Hill, Advance in Oxygenated Process, JAI, London, 1998.
9. R. C. Larock, Comprehensive Organic Transformations, VCH, New York, 1989.
10. K. Mori, S. Kanai, T. Hara, T. Mizugaki, K. Ebitani, K. Jitsukawa and K. Kaneda, *Chem. Mater.*, 2007, **19**, 1249.
11. T. Mallat and A. Baiker, *Chem. Rev.*, 2004, **104**, 3037.
12. C. Parmeggiani and F. Cardona, *Green Chem.*, 2012, **14**, 547.

13. C. P. Vinod, K. Wilson and F. Lee, *J. Chem. Technol. Biotechnol.*, 2011, **86**, 161.

14. X. M. Wang, G. J. Wu, N. J. Guan and L. D. Li, *Appl. Catal., B*, 2012, **115–116**, 7.

15. Y. Su, L. C. Wang, Y. M. Liu, Y. Cao, H. Y. He and K. N. Fan, *Catal. Commun.*, 2007, **8**, 2181.

16. Y. Chen, H. Wang, C. J. Liu, Z. Zeng, H. Zhang, C. Zhou, X. Jia, Y. Yang, *J. Catal.*, 2012, **289**, 105.

17. T. Punniyamurthy and L. Rout, *Coord. Chem. Rev.*, 2008, **252**, 134.

18. L. Guidoni, K. Spiegel, M. Zumstein and U. Rothlisberger, *Angew. Chem.*, 2004, **116**, 3348; *Angew. Chem. Int. Ed.*, 2004, **43**, 3286.

19. (a) P. Chaudhuri, M. Hess, U. Flörke and K. Wieghardt, *Angew. Chem., Int. Ed.*, 1998, **37**, 2217; (b) I. E. Markó, A. Gautier, R. L. Dumeunier, K. Doda, F. Philippart, S. M. Brown and C. J. Urch, *Angew. Chem., Int. Ed.*, 2004, **43**, 1588; (c) C. J. Gartshore and D. W. Lupton, *Adv. Synth. Catal.*, 2010, **352**, 332; (d) Y. Zhu, B. Zhao and Y. Shi, *Org. Lett.*, 2013, **15**, 992.

20. (a) M. F. Semmelhack, C. R. Schmid, D. A. Cortés and C. S. Chou, *J. Am. Chem. Soc.*,1984, **106**, 3374; (b) G. Ragagnin, B. Betzemeier, S. Quici and P. Knochel, *Tetrahedron*, 2002, **58**, 3985; (c) P. Gamez, I. W. C. E. Arends, J. Reedijk and R. A. Sheldon, *Chem. Commun.*, 2003, **2414**; (d) P. Gamez, I. W. C. E. Arends, R. A. Sheldon and J. Reedijk, *Adv. Synth. Catal.*, 2004, **346**, 805; (e) N. Jiang and A. Ragauskas, *J. Org. Lett.*, 2005, **7**, 3689; (f) N. Jiang and A. J. Ragauskas, *J. Org. Chem.*, 2006, **71**, 7087; (g) S. Mannam, S. K. Alamsetti and G. Sekar, *Adv. Synth. Catal.*, 2007, **349**, 2253; (h) J. M. Hoover and S. S. Stahl, *J. Am. Chem. Soc.*, 2011, **133**, 16901; (e) X. Liu, Q. Xia, Y. Zhang, C. Chen and W. Chen, *J. Org. Chem.*, 2013, **78**, 8531; (f) I. Gamba, I. Mutikainen, E. Bouwman, J. Reedijk and S. Bonnet, *Eur. J. Inorg. Chem.*, 2013, **115**.

21. a) A. Hu, G. T. Yee and W. Lin, *J. Am. Chem. Soc.*, 2005, **127**, 12486; (b) N. T. S. Phan, C. S. Gill, J. V. Nguyen, Z. J. Zhang and C.W. Jones, *Angew. Chem., Int. Ed.*, 2006, **45**, 2209; (c) R. Abu-Reziq, H. Alper, D. Wang and M.

L. Post, *J. Am. Chem. Soc.*, 2006, **128**, 5279; (d) C. O. Dalaigh, S. A. Corr, Y. Gunko and S. J. Connon, *Angew. Chem., Int. Ed.*, 2007, **46**, 4329; (e) T. Hara, T. Kaneta, K. Mori, T. Mitsudome, T. Mizugaki, K. Ebitanic and K. Kaneda, *Green Chem.*, 2007, **9**, 1246;(f) A.-H. Lu, E. L. Salabas and F. Schuth, *Angew. Chem., Int. Ed.*, 2007, **46**, 1222; (g) A. H. Latham and M. E.Williams, *Acc. Chem. Res.*, 2008, **41**, 411.

22. N. T. S. Phan and C. W. Jones, *J. Mol. Catal. A: Chem.*, 2006, **253**, 123.
23. F. Zamani, S. M. Hosseini and S. Kianpour, *Dalton Trans.*, 2014, DOI: 10.1039/c3dt52729h
24. (a) B. Li, L. Gao, F. Bian and W. Yu, *Tetrahedron Lett.*, 2013, **54**, 1063; (b) X. Jin, K. Zhang, J. Sun, J. Wang, Z. Dong and R. Li, *Catal. Commun.*, 2012, **26**, 199 ; (c) M. Esmaeilpour, A. R. Sardarian and J. Javidi, *Appl. Catal., A*, 2012, **445–446**, 359; (d) G. M. Ucoski, F. S. Nunes, G. DeFreitas-Silva, Y. M. Idemori and S. Nakagaki, *Appl. Catal., A*, 2013, **459**, 121; (e) R. K. Sharma, Y. Monga, A. Puri and G. Gaba, *Green Chem.*, 2013, **15**, 2800.
25. (a) S. Wu, Q. He, C. Zhou, X. Qi, X. Huang, Z. Yin, Y. Yang and H. Zhang, *Nanoscale*, 2012, **4**, 2478; (b) M. Kotani, T. Koike, K. Yamaguchia, N. Mizuno, *Green Chem.*, 2006, **8**, 735; (c) J. Zhu, P. Wang and M. Lu, *J. Braz. Chem. Soc.*, 2013, **24**, 171; (d) F. Shi, M. K. Tse, M-M. Pohl, J. Radnik, A. Brückner, S. Zhang and M. Beller *J. Mol. Catal. A: Chem.*, 2008, **292**, 28; (e) R. L. Oliveira, P. K. Kiyohara and L. M. Rossi, *Green Chem.*, 2010, **12**, 144.
26. (a) P. S Rathore, J. Advani, S. Rathore and S. Thakore, *J Mol Catal A: Chem*, 2013, **377**, 129; (b) P. S Rathore, R. Patidar, S. Rathore and S. Thakore, *Catal Lett*, 2013, **144**, 439.
27. V. Polshettiwar and R. S. Varma, *Org. Biomol. Chem.*, 2009, **7**, 37.
28. E. Karaoğlu, A. Baykal, M. Senel, H. Sözeri and M. S. Toprak, *Mater. Res. Bull.*, 2012, **47**, 2480.
29. L. Cabrera, S. Gutierrez, M. P. Morales, N. Menendez and P. Herrasti, *J. Magn. Magn. Mater.*, 2009, **321**, 2115.
30. H. Deng and Z. Lei, *Composites, Part B*, 2013, **54**, 194.
31. H. Mart, *J Macromol Sci, Pure Appl Chem*, 2005, **42**, 1197.

32. M. C. Biesinger, L.W. M. Lau, A. R. Gerson and R. St.C. Smart, *Appl. Surf. Sci.*, 2010, **257**, 887.

(Spectral Data)

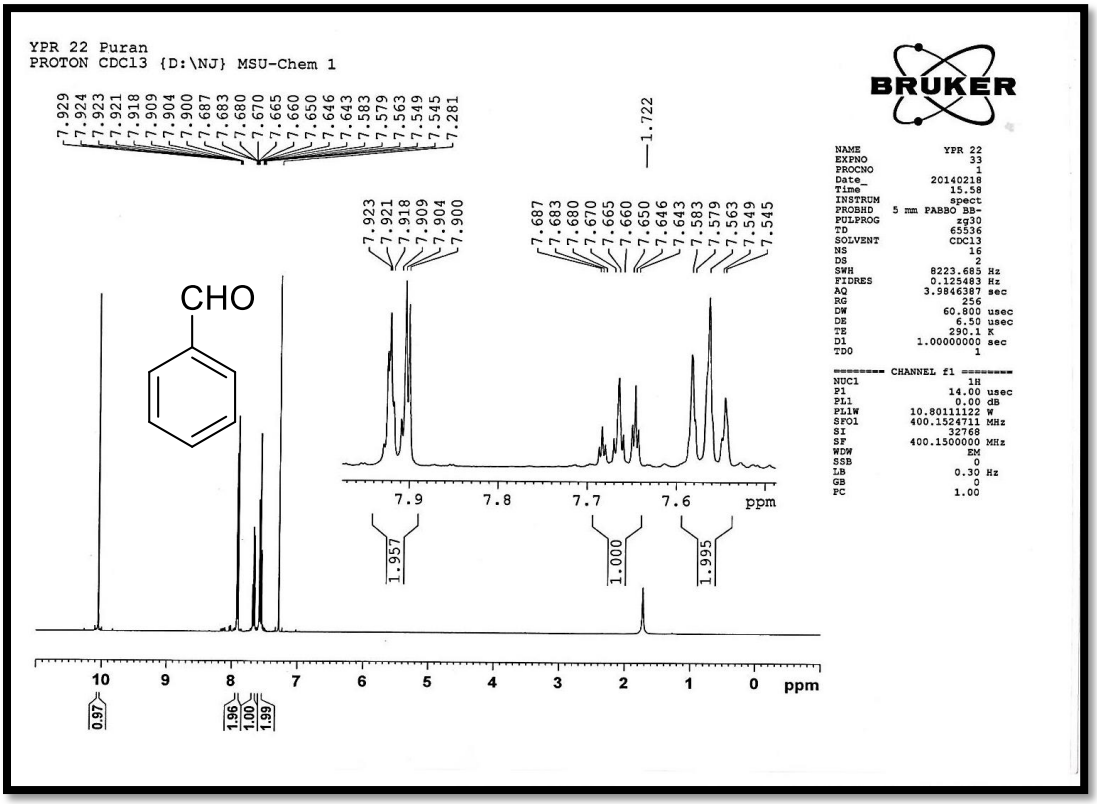

Figure S1 ^{1}HNMR spectra of benzaldehyde ($CDCl_3$, Table-5.4, Entry-1)

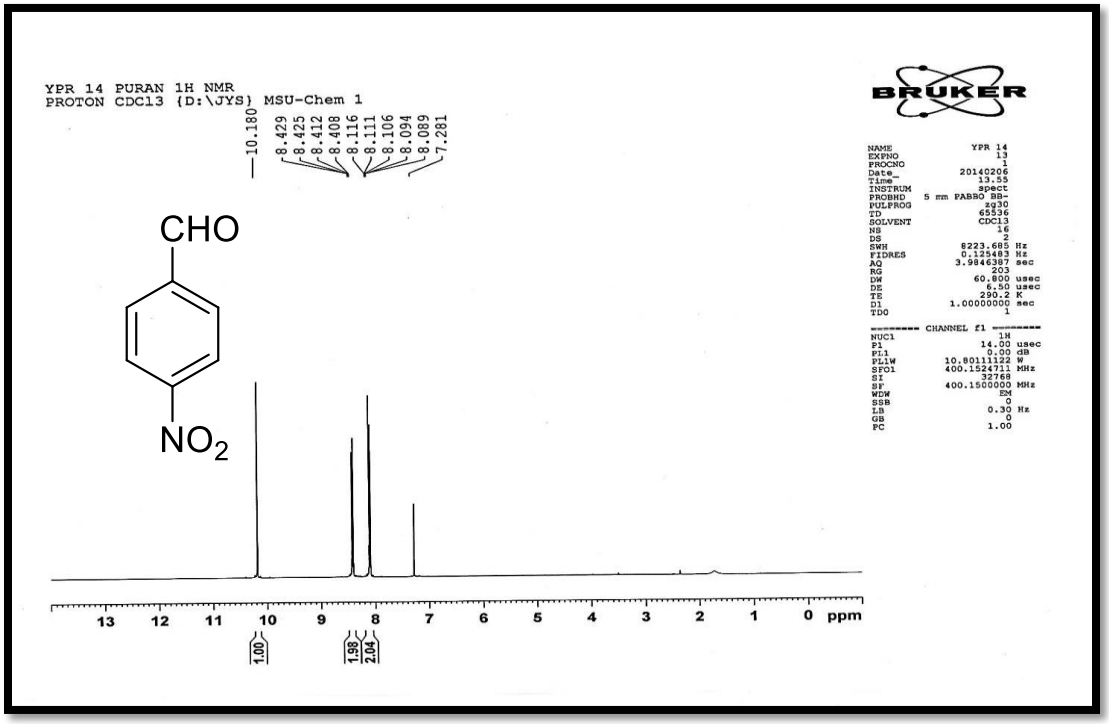

Figure S2 ^{1}HNMR spectra of 4-nitrobenzaldehyde ($CDCl_3$, Table-5.4, Entry-2)

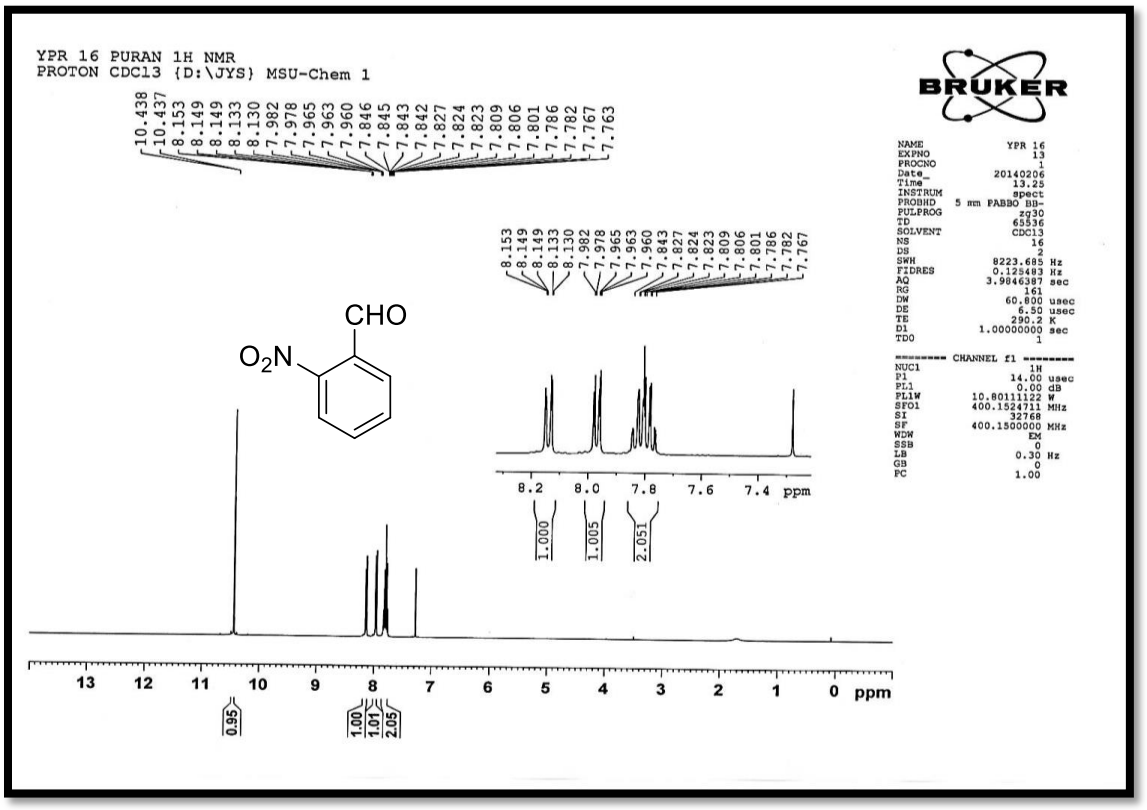

Figure S3 ^{1}HNMR spectra of 2-nitrobenzaldehyde ($CDCl_3$, Table-5.4, Entry-3)

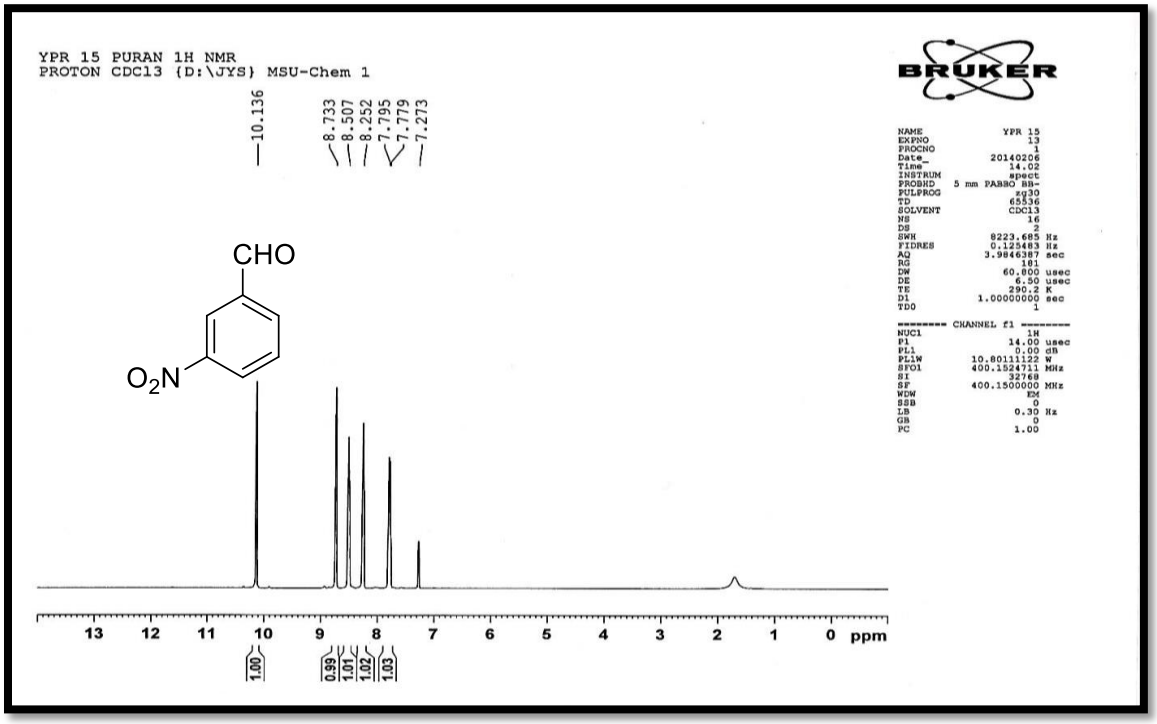

Figure S4 ^{1}HNMR spectra of 3-nitrobenzaldehyde ($CDCl_3$, Table-5.4, Entry-4)

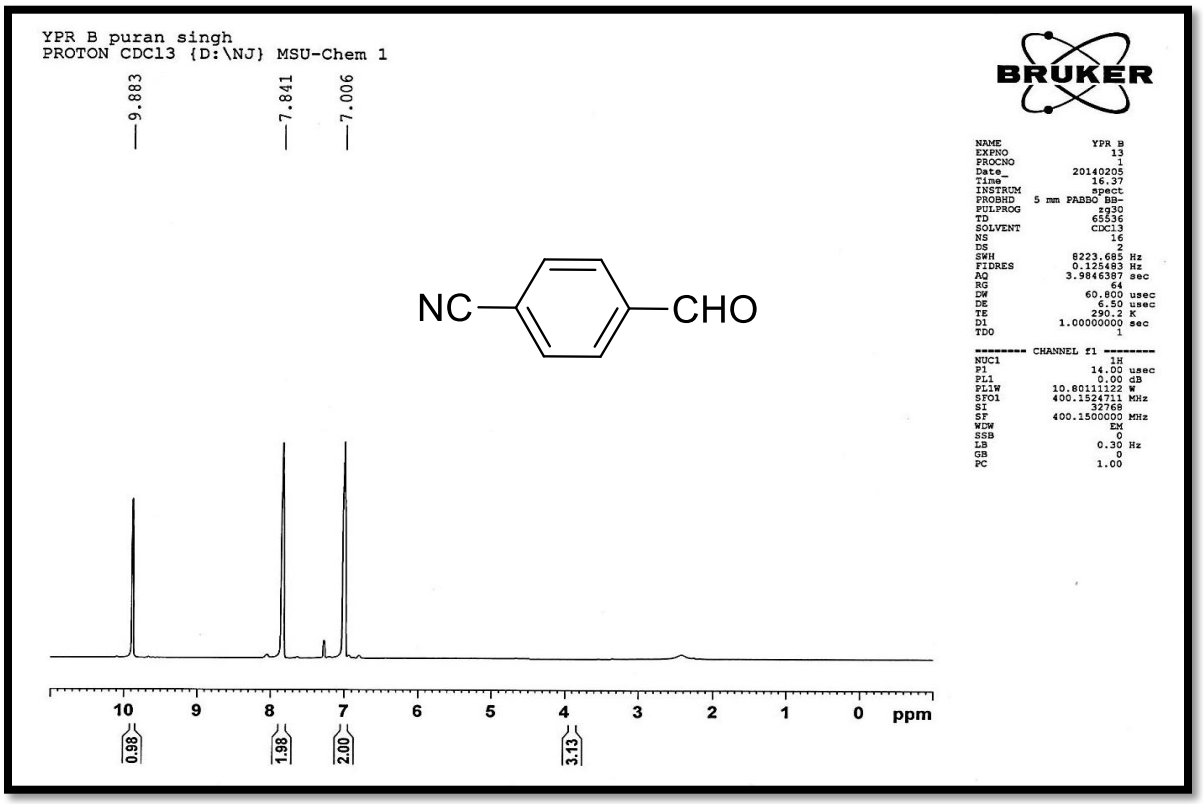

Figure S5 ^{1}HNMR spectra of 4-cynobenzaldehyde ($CDCl_3$, Table-5.4, Entry-5)

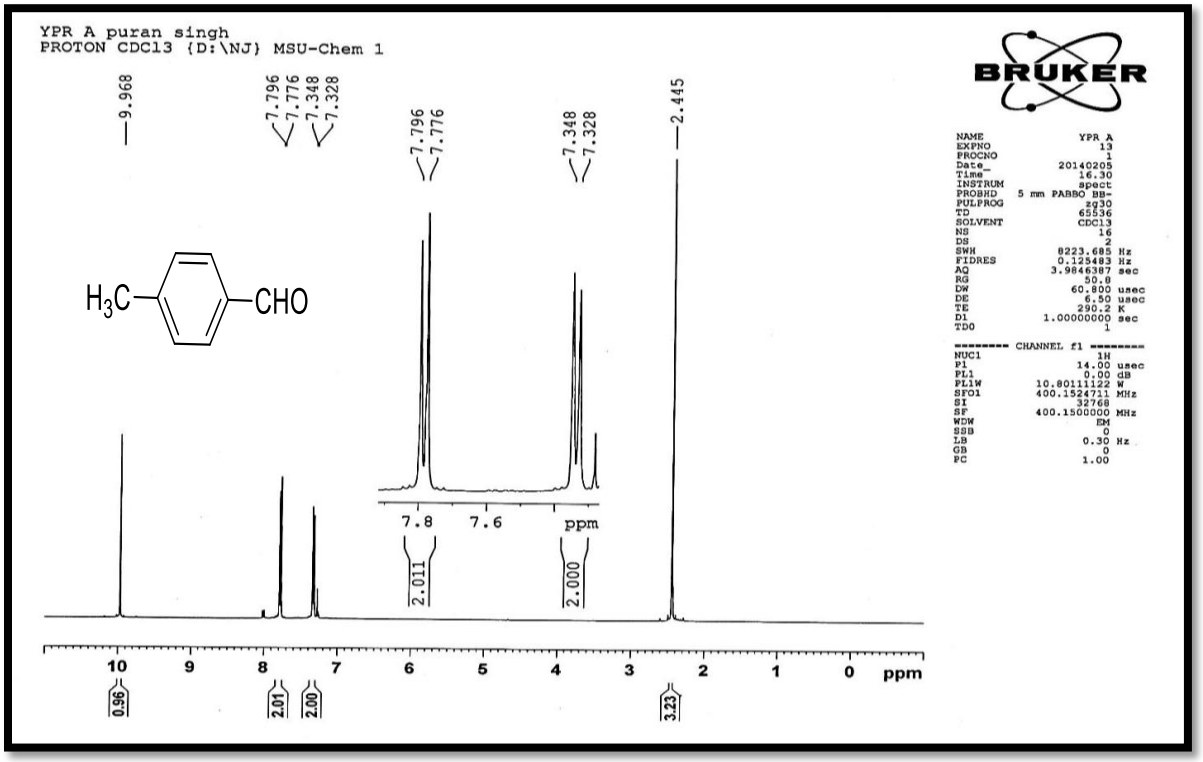

Figure S6 ^{1}HNMR spectra of 4-methylbenzaldehyde ($CDCl_3$, Table-5.4, Entry-6)

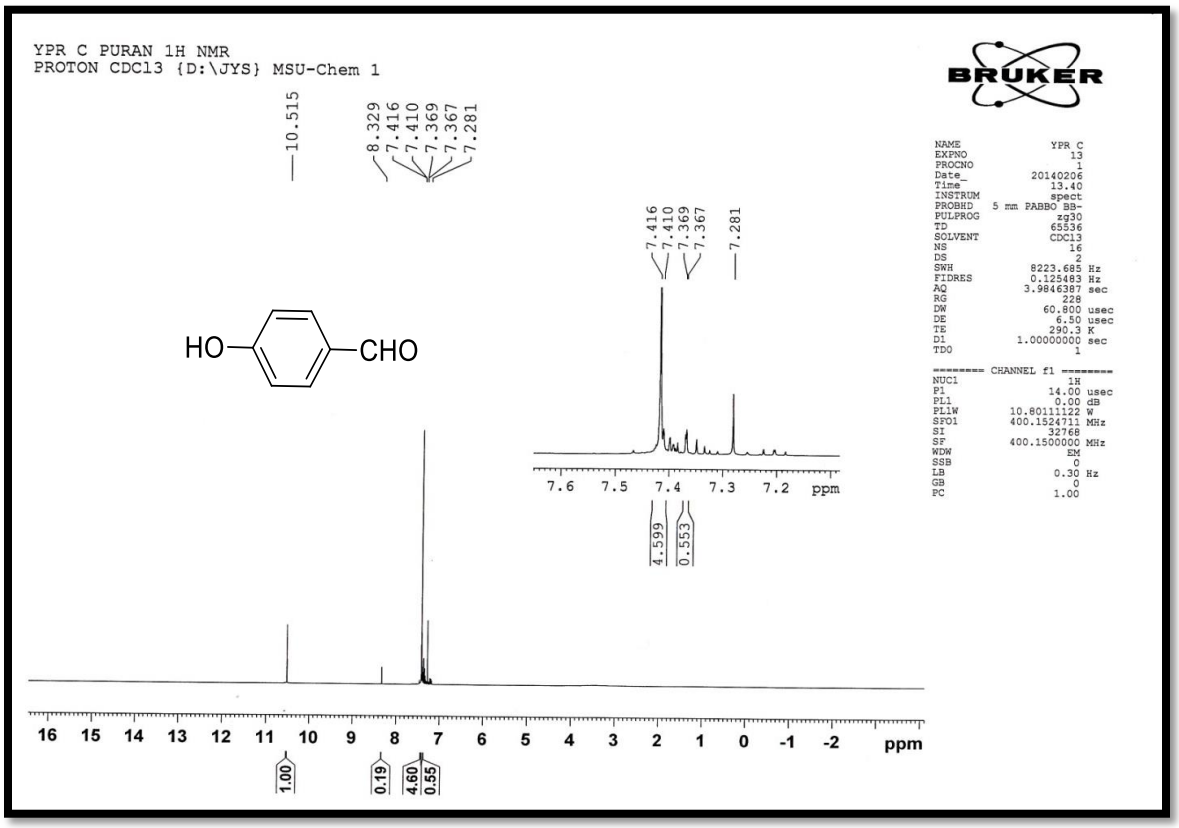

Figure S7 [1]HNMR spectra of 4-hydroxybenzaldehyde ($CDCl_3$, Table-5.4, Entry-7)

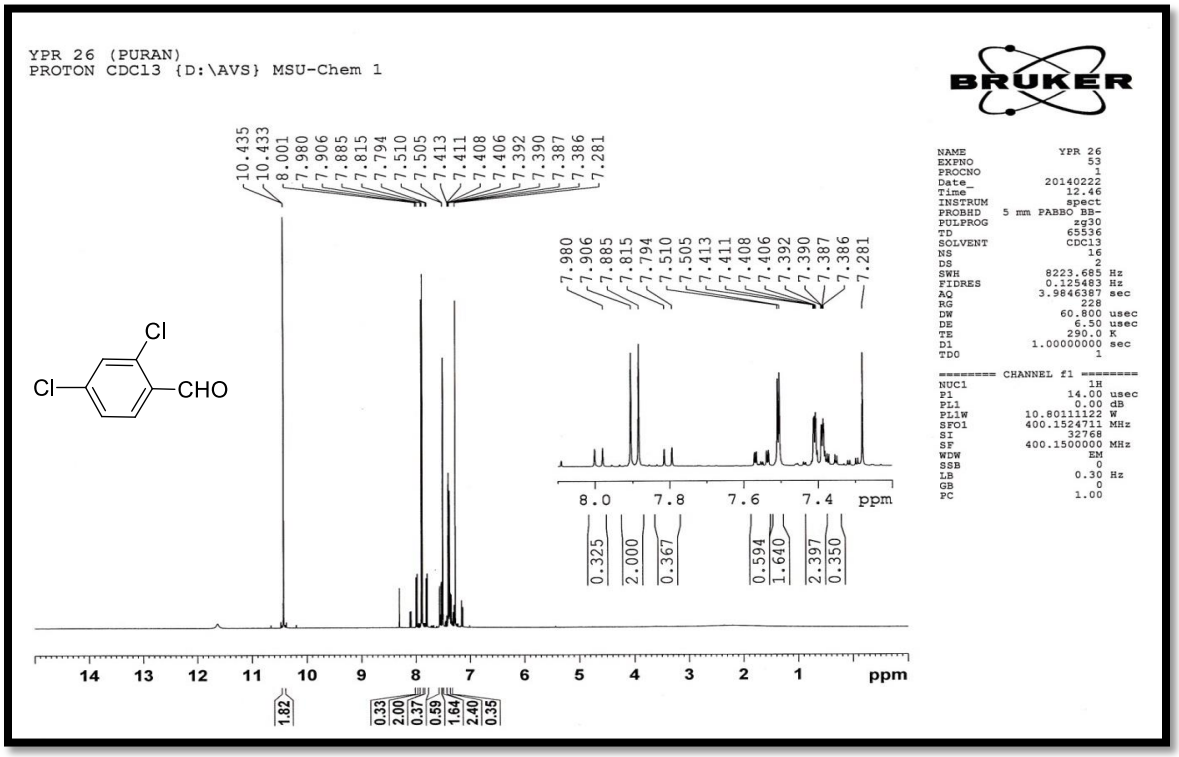

Figure S8 [1]HNMR spectra of 2,4-dichlorobenzaldehyde ($CDCl_3$, Table-5.4, Entry-8)

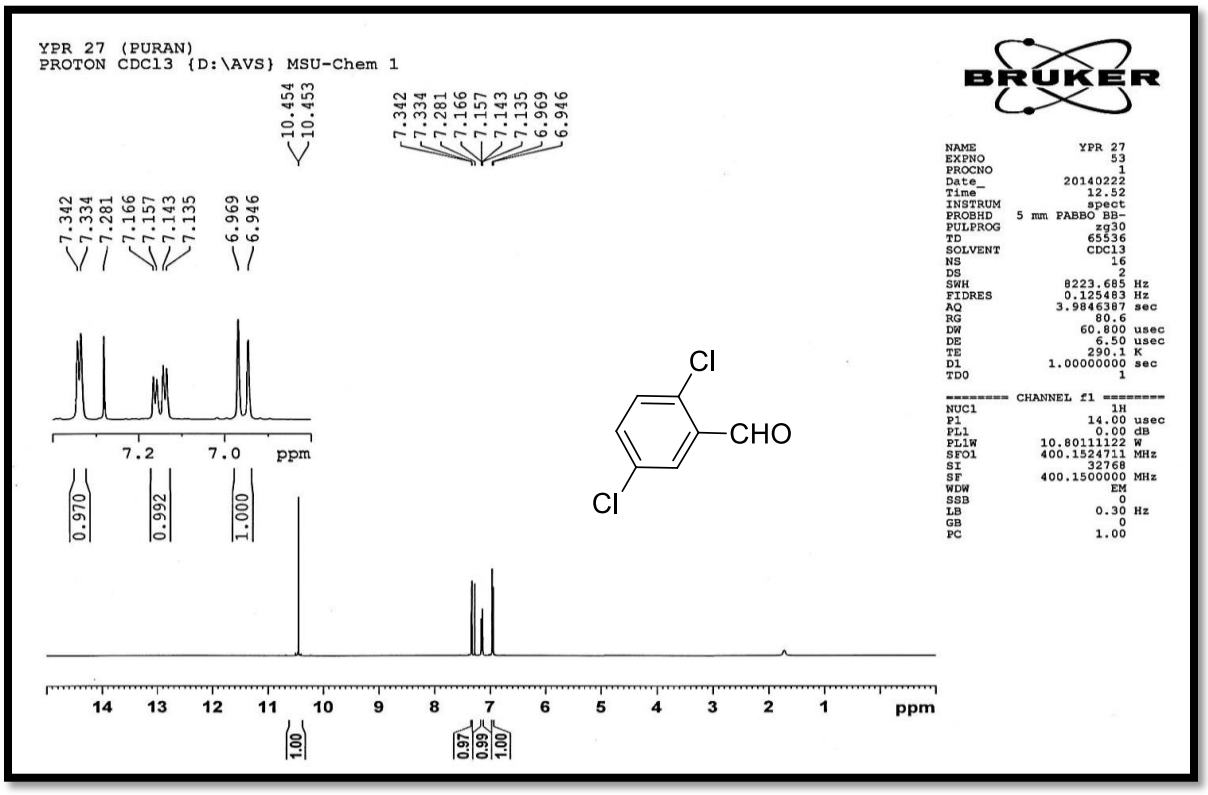

Figure S9 [1]HNMR spectra of 2,5-dichlorobenzaldehyde ($CDCl_3$, Table-5.4, Entry-9)

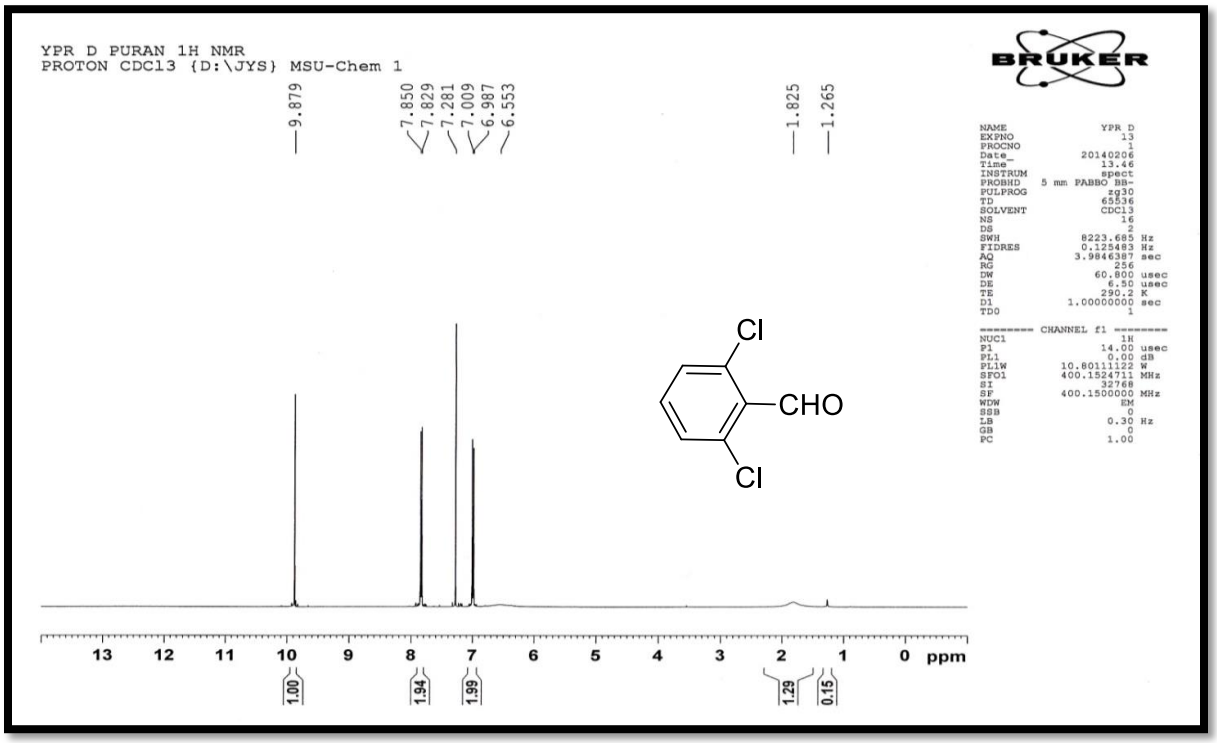

Figure S10 [1]HNMR spectra of 2,6-dichlorobenzaldehyde ($CDCl_3$, Table-5.4, Entry-10)

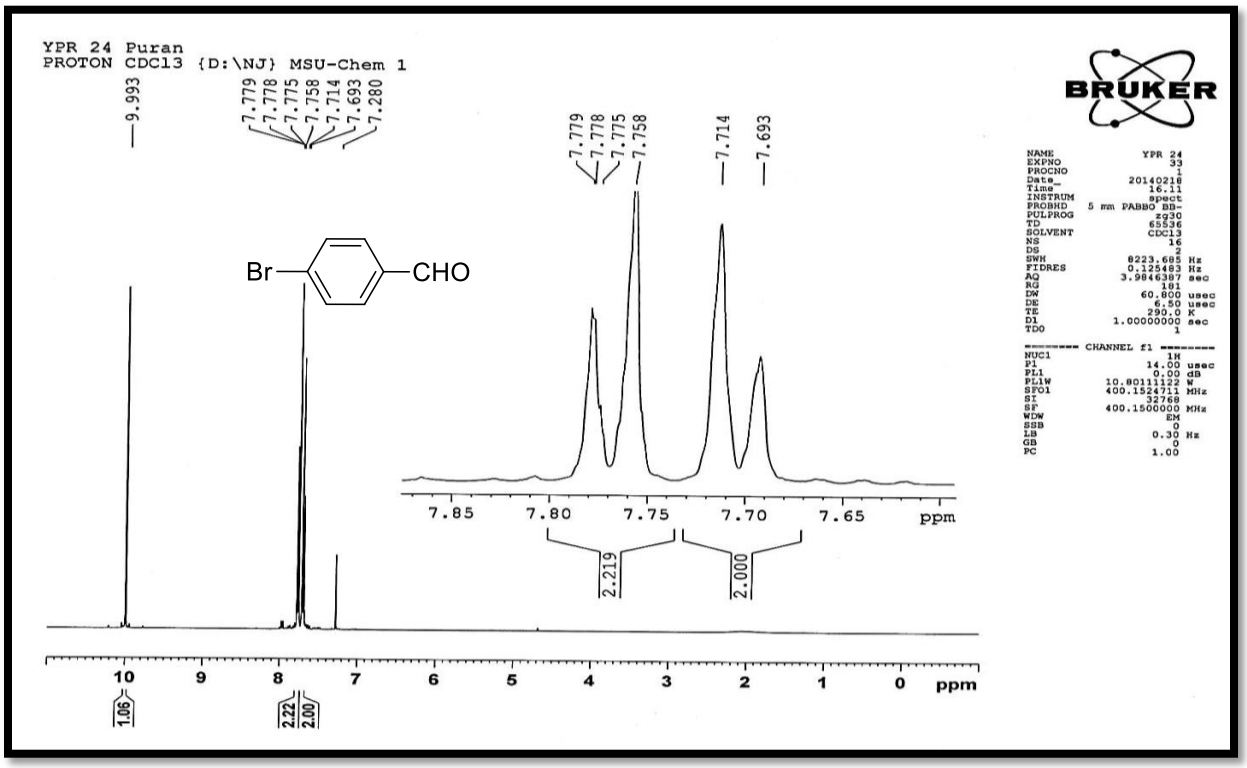

Figure S11 ^{1}HNMR spectra of 4-bromobenzaldehyde ($CDCl_3$, Table-5.4, Entry-11)

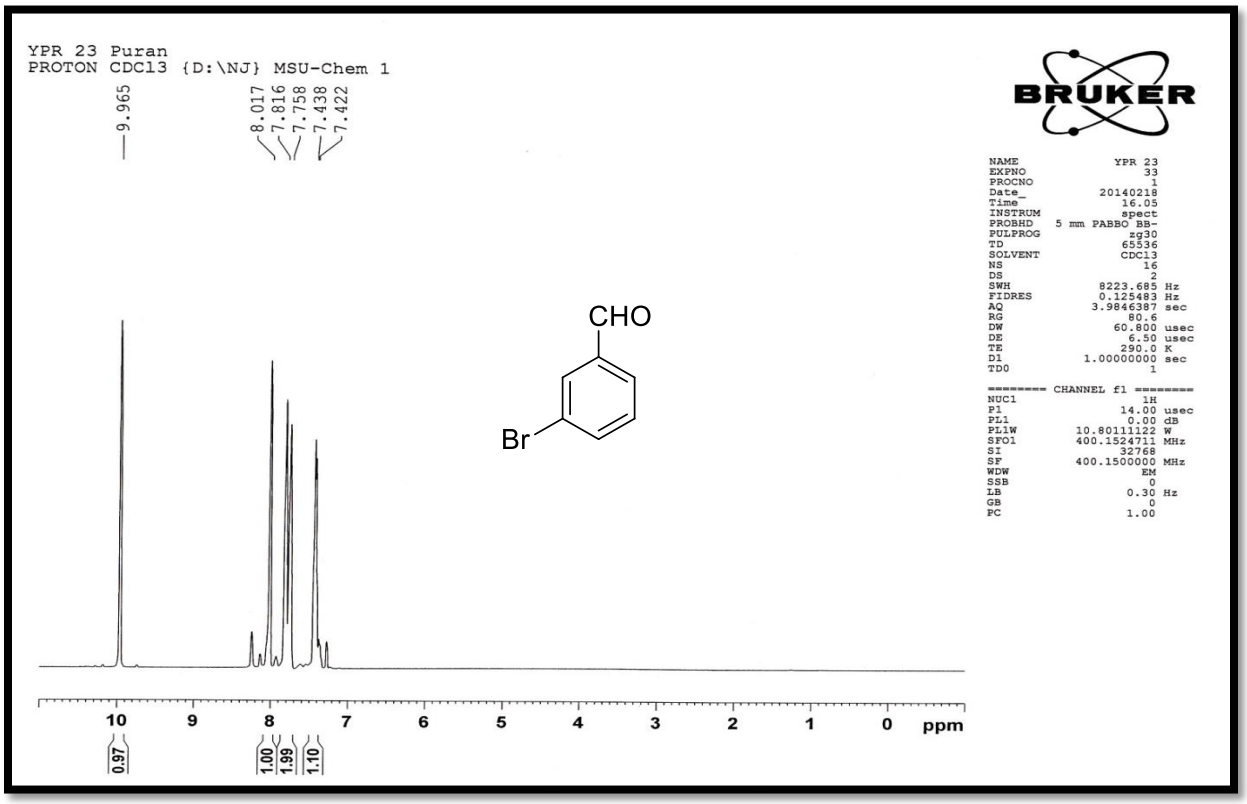

Figure S12 ^{1}HNMR spectra of 3-bromobenzaldehyde ($CDCl_3$, Table-5.4, Entry-12)

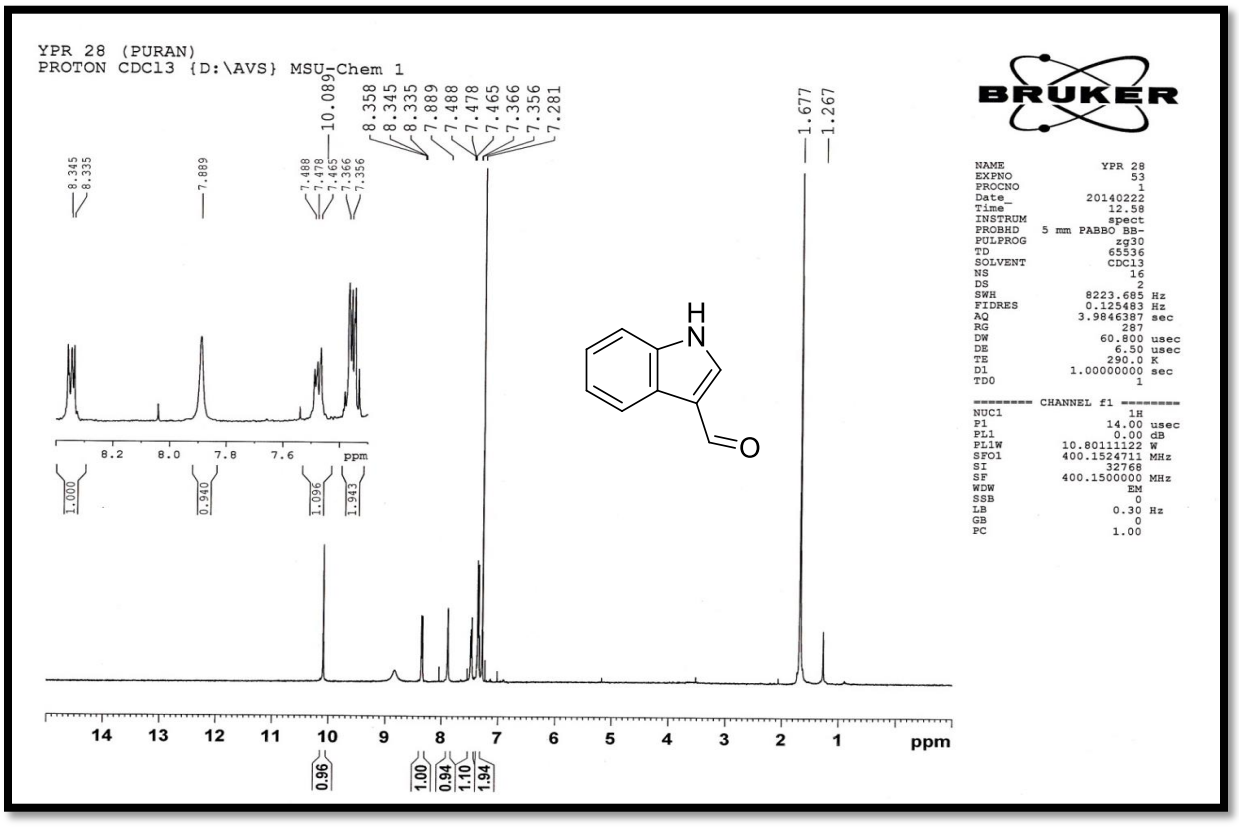

Figure S13 ^{1}HNMR spectra of Indole-3-carboxyaldehyde ($CDCl_3$, Table-5.4, Entry-13)